# Measurement of the Nonlinear Refractive Index in the High Laser Intensity Limit

**Ashwaq Hakami**

Thesis submitted to the

Faculty of Graduate and Postdoctoral Studies

in partial fulfillment of the requirements for the degree of

M. Sc. in Physics

Supervised by

Prof. Thomas Brabec

Ottawa Carleton Institute of Physics

Department of Physics

University of Ottawa

Ottawa, Canada

# Abstract

When an intense laser beam interacts with matter, the Kerr nonlinearity results in self-focusing. Above the critical intensity, self-focusing dominates pulse spreading through diffraction leading to continuous pulse narrowing and thus an increase of the laser peak intensity. Collapse is prevented through the fact that peak intensities ultimately reach a level where ionization occurs. The profile of ionized electrons represents a negative lens which balances Kerr nonlinear self-focusing and causes the formation of stable filaments. From filaments radiation is emitted in a cone around the filament which has been termed conical emission. Filament formation happens at non-perturbative intensities where the formalism of perturbative nonlinear optics loses its validity. This opens the question of how the Kerr nonlinearity behaves in the non-perturbative limit and how large the Kerr nonlinear coefficient is.

The expression for the Kerr nonlinearity is derived by perturbation theory; the validity of this expression in the non-perturbative limit is questionable. Further, experimentally the Kerr nonlinear index is extracted from measurements of the self-focusing distance as a function of beam intensity which is called the Z-scan method. This method fails at non-perturbative intensities due to the presence of the negative lens coming from the ionized electrons. The effects of the positive focusing and negative self-defocusing lens cannot be separated by the Z-scan method. As a result, not much is known about the Kerr nonlinearity in the regime of non-perturbative nonlinear optics.

The purpose of this thesis is twofold. First, recently it has been discovered that conical emission can be utilized as a broadband and very efficient amplification mechanism in the far infrared. The process has been dubbed Kerr instability amplification. The difference between conical emission and Kerr instability amplification is that they take place in two different regimes of the nonlinear interaction. Whereas conical emission grows out of noise and therewith only takes place once the pump pulse has been substantially restructured due to filamentation, Kerr instability amplification is seeded with a second pulse and therewith occurs long before filamentation happens. The theory developed for Kerr instability amplification has been developed based on a stability analysis of the scalar wave equation. This analysis has shown that with pump lasers in the 1-2 $\mu$m range amplification of infrared radiation up to the 10's of $\mu$m can be achieved.

For amplification over such a wide range it is not adhoc clear to which exent vectorial wave effects can be neglected. The first part of the thesis closes this gap by developing the vectorial theory of vector instability amplification.

The second part uses the results derived for Kerr instability amplification to answer the question of how to measure the Kerr nonlinear index in the nonperturbative laser intensity limit. The idea rests on the fact that Kerr instability amplification is maximum for a specific angle between pump and seed beam which varies as a function of laser pump intensity. A relation is derived that connects this angle with the Kerr nonlinear refractive index. As a result, from the maximum angle measured as a function of pump intensity, both magnitude and functional form of the Kerr nonlinear index as a function of laser intensity can be determined.

## Acknowledgement

First and above all, I would like to thank God Almighty for giving me the knowledge, strength, ability and opportunity to conduct this research study and to proceed successfully. Without his blessings, this accomplishment would not have been possible. I offer my honest gratitude to my supervisor, Dr. Thomas Brabec, who has supported me thoughout my thesis with his patience and knowledge throughout my time as his student . I have been extremely lucky to have a supervisor who cared so much about my work. His guidance helped me in all the time of research and writing of this thesis. I am grateful to Michael Nesrallah for helping me understand the research. Words cannot express my gratitude and appreciation to my mother,Hajriyyah Hakami,and father Hamoud Hakami, I warmly thank and appreciate my parents. You are always there for me. I also would like to thank my brothers, sisters for they have provided assistance in various ways. Finally, To all my friends, thank you for your understanding and encouragement in my many moments of crisis.

# Contents

# List of Figures

# Chapter 1

# Introduction

In the following a brief introduction into nonlinear optics is given with emphasis on the Kerr nonlinearity. The Kerr nonlinearity is responsible for a rich set of physical phenomena ranging from self-focusing and self phase modulation to conical emission and filamentation. These phenomena are used for a wide range of applications in photonics and have been and still are subject to intense research.

Self phase modulation is the main process for spectral widening. In combination with negative group velocity dispersion this results in temporal shortenting of laser pulses. Self phase modulation and negative dispersion alone are not sufficent to create stable femtosecond pulses in ultrafast resonators [1]. The presence of self-focusing in combination with an aperture is needed to stabilize ultrashort pulse generation. Further, self-focusing is important for applications such as optical switching of pulses in fiber optics and telecommunications.

The fact that the Kerr nonlinearity exhibits unstable behavior and breakup of pulses is of direct relevance for this work. In fibers, which are one-dimensional systems, the Kerr instability is known as modulation instability. When a plane wave propagates down a fiber, the Kerr instability leads to a breakup of the plane wave into a spectrum of frequencies which grow out of noise [2]. In three-dimensional systems, such as bulk materials, liquids and gases, the Kerr instability results in a break up of the transverse part of

the pulse into a single or multiple filaments. At the extreme intensities occurring during filamentation the form and magnitude of the Kerr nonlinearity are not well understood.

Filamentation is currently an active area of research because of various attractive properties. The fact that a filament can propagate over long distances without diffraction is used for remote sensing [3]. A filament is sent up into the atmosphere and from measurements of the reflected signal the composition of the atmosphere at high altitudes can be explored. Further, filaments are being used to remotely monitor extreme processes, such as nuclear explosions, where conventional sensors fail to work [4]. Finally, filaments are also being used in weather formation experiments. It has been shown that filaments can trigger lightening and even snow condensation [5]. Filamentation is also accompanied by the conical emission of a wide range of optical frequencies ranging from the uv to the near infrared; conical emission grows out of noise [6] arising from vacuum flucuations. Recently, seeding the Kerr instability with a second pulse has been investigated for the first time. It has been found that this process can be used for Kerr instability amplification of single-cycle pulses over a wide range of frequencies from the uv to mid-infrared frequencies beyond $10\mu$m [7]. These mechanisms have been termed Kerr instability amplification (KIA).

The goal of this thesis is twofold. First, the original theory [7] has been developed from a stability analysis of the nonlinear scalar wave equation. It is not adhoc clear how good the scalar approximation is. Here, I develop a vector theory of KIA which proves that vectorial effects are negligible over the whole spectral range of amplification.

The results from this theory are used in the second part to better understand the Kerr nonlinearities at extreme intensities. I show how KIA experiments can be used to measure the functional form and the magnitude of the Kerr nonlinear index.

## 1.1 Nonlinear Optics

The response of matter to light is characterized by the polarization $\mathbf{P}$. At low laser intensities, the relation between the light electric field $\mathbf{E}$ and the polarization response $\mathbf{P}$ is linear,

$$\mathbf{P} = \epsilon_0 \chi^{(1)} \mathbf{E}, \tag{1.1}$$

where $\epsilon_0$ is the permittivity of free space. The linear susceptibility $\chi^{(1)}$ defines the dielectric constant $\epsilon$ and the linear refractive index $n$ via the relation $\epsilon = \epsilon_0(1 + \chi^{(1)}) = n^2$. Note that in general linear susceptibility and refractive index are frequency dependent. As a result, Eq.(1.1) becomes

$$\mathbf{P}(t) = \epsilon_0 \int_{-\infty}^{t} dt' \chi^{(1)}(t - t')\mathbf{E}(t'). \tag{1.2}$$

By using the Fourier transform

$$\mathbf{E}(\omega) = \frac{1}{\sqrt{2\pi}} \int_{-\infty}^{\infty} dt' \mathbf{E}(t') e^{i\omega t'} \tag{1.3}$$

The linear polarization relation (1.2) can be written as

$$\mathbf{P}(\omega) = \epsilon_0 \chi^{(1)}(\omega)\mathbf{E}(\omega) \tag{1.4}$$

At higher laser intensities around $I = 10^7 - 10^8$ W/cm $^2$ the response of matter to light becomes nonlinear where higher powers of $\mathbf{E}$ are non-negligible in $\mathbf{P}(\omega)$. Here, the electric field is defined as

$$\mathbf{E} = \hat{x} E_0 F(\mathbf{x}, t) e^{-i\omega_0 t + ik_0 z} + c.c., \tag{1.5}$$

where peak field strength $E_0$ and peak intensity $I_0$ are related by $I_0 = 2n_0/Z_0 E_0^2$; $Z_0 = \sqrt{\mu_0/\epsilon_0}$ represents the free space impedance where $\mu_0$ is the impedance of free space, and $n_0 = n(\omega_0)$ is the refractive index at the center frequency of the laser pulse, $\omega_0$. Further, the laser wavevector points along $\hat{z}$ and is defined as $k_0 = k(\omega_0) = n_0\omega_0/c$ and the laser is polarized along unit vector $\hat{\boldsymbol{x}}$. Finally, $F$ is the pulse envelope and

$\mathbf{x} = (x, y, z)$ is the space coordinate.

As long as the nonlinear contributions to the polarization are much smaller than the linear ones, the polarization $\mathbf{P}$ can be expanded in a Taylor series which gives

$$\begin{aligned}\mathbf{P}(t) &= \epsilon_0(\chi^{(1)}\mathbf{E} + \chi^{(2)}\mathbf{E}^2 + \chi^{(3)}\mathbf{E}^3 + .....) \\ &\equiv \mathbf{P}^{(1)}(t) + \mathbf{P}^{(2)}(t) + \mathbf{P}^{(3)}(t) + .....\end{aligned} \tag{1.6}$$

The quantities $\chi^{(2)}$ and $\chi^{(3)}$ are known as the second- and third-order non-linear optical susceptibilities. For the sake of simplicity they are assumed scalars from here onwards which is valid for linearly polarized light, although in their most general form they are represented by tensors. As a result, all polarization terms are directed along the laser electric field polarization in Eq.(1.5). The terms $\mathbf{P}^{(2)}(t) = \epsilon_0\hat{x}\chi^{(2)}\mathbf{E}^2$ and $\mathbf{P}^{(3)} = \epsilon_0\chi^{(3)}\mathbf{E}^3$ are referred to as second-order nonlinear polarization and third-order nonlinear polarization, respectively.

The physical processes occurring as a result of second and third-order nonlinear polarizations are quite distinct. Second-order nonlinear optical interactions can happen only in noncentrosymmetric crystals that means in crystals that do not display inversion symmetry. As the response along the positive and negative electric field cycles have the same magnitude and just opposite sign, $\chi^{(2)}$ vanishes identically for inversion symmetric materials.

To better understand the different types of optical responses we insert the electric field Eq.(1.5) into the expression for $\mathbf{P}^{(2)}$ which yields

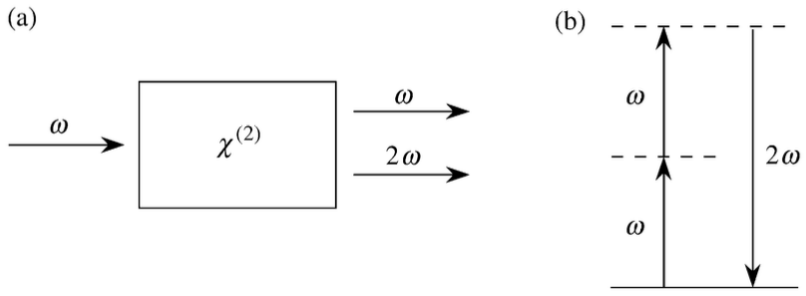


*Figure 1.1: (a) Geometry of second-harmonic generation. (b) Energy-level diagram describing second-harmonic generation [8].*

$$\mathbf{P}^{(2)} = 2\hat{\mathbf{x}}\epsilon_0\chi^{(2)}E_0^2|F(t)|^2 + \hat{\mathbf{x}}(\epsilon_0\chi^{(2)}E_0^2F(t)^2e^{-2i\omega_0t+2ik_0z} + c.c.) \tag{1.7}$$

The first term represents optical rectification which is one of the main processes to generate long wavelength (THz) radiation [9]. The second term creates a field with double the frequency of the pump pulse, which is referred to as second harmonic generation, see Fig.(1.1). As an example, second harmonic generation is used to generate higher frequency fields in the ultraviolet. Related to second harmonic generation is optical parametric oscillation and amplification where a field with photon frequency $\omega_0 = \omega_1 + \omega_2$ decays into two field with smaller frequencies $\omega_1$ and $\omega_2$. This process finds frequent use in the generation and amplification of mid-infrared radiation fields. In quantum optics, it is used to generate correlated (entangled) pairs of photons [10] for fundamental quantum experiments.

We next look at the third-order contribution to the nonlinear polarization and insert the electric field ansatz (1.5) into it, resulting in

$$\mathbf{P}^{(3)} = \hat{\mathbf{x}}\epsilon_0\chi^3E_0^3\left[F(t)^3e^{-3i\omega_0t+3ik_0z} + 3|F(t)|^2F(t)e^{-i\omega_0t+ik_0z} + c.c.\right]. \tag{1.8}$$

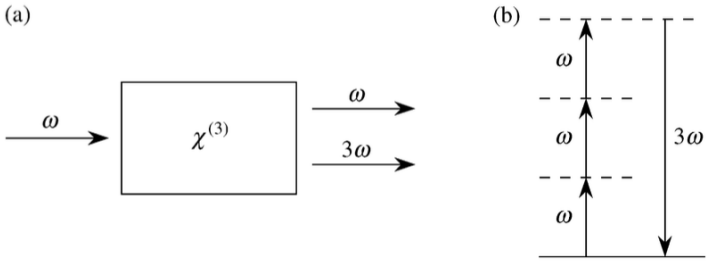


*Figure 1.2: Third-harmonic generation, (a) Geometry of the interaction, (b) Energy-level description [8].*

In the third order susceptibility term three photons are combined to obtain a fourth photon; this is a special case of the more general four wave mixing process, see Fig.(1.2). If three different pump photon frequencies are used the third order nonlinearity is referred to as four wave mixing. The first term in Eq.(1.8) is called third harmonic generation and the second term refers to the Kerr nonlinearity which is the main subject of this investigation. Third-order nonlinear optical interactions can happen for both centrosymmetric and noncentrosymmetric media.

The response of an atom is governed by the atomic electric field strength $E_{at} = e(4\pi\epsilon_0 a_0^2)^{-1} = 5.14 \times 10^{11}$ V/m, which is the field strength of the nucleus experienced by an electron in its atomic ground state. Here $e$ is the charge of the electron, $a_0 = 4\pi\epsilon_0\hbar^2/(me^2)$ is the Bohr radius of the hydrogen atom, $\hbar$ is Plancks constant, and $m$ is the mass of the electron. It is reasonable to assume that when the laser field becomes comparable to the atomic field strength, the polarization terms in the Taylor expansion become comparable and the Taylor expansion loses its validity. This is the realm of non-perturbative optics and in practice it starts at intensities of about $10^{13} - 10^{14}\mathrm{W/cm}^2$, where ionization becomes dominant.

The time−varying polarization $\mathbf{P}(t)$ in Eq.(1.6) acts as a source or generating new components of the electromagnetic field. The generation and evolution of these new electric field components is governed by inserting Eq.(1.6) into Maxwell's equations. After eliminating the magnetic field we obtain the vector wave equation

$$\nabla^2\widetilde{\mathbf{E}} - \boldsymbol{\nabla}(\boldsymbol{\nabla}\cdot\mathbf{E}) - \frac{n^2}{c^2}\frac{\partial^2\mathbf{E}}{\partial t^2} = \frac{1}{\epsilon_0 c^2}\frac{\partial^2\mathbf{P}^{nl}}{\partial t^2}. \tag{1.9}$$

Here, $c$ is the vacuum light velocity and the polarization has been split into a linear part and a nonlinear part

$\mathbf{P}^{nl}$. The linear part results in the term with the linear refractive index on the left hand side of Eq.(1.9).

## 1.2 Kerr Nonlinearity.

After this brief introduction into general nonlinear optics we focus on a more in depth discussion of the Kerr nonlinearity. The second term in Eq.(1.8) can be written as

$$n_2 I_0 |F|^2 \hat{x} E_0 F e^{-i\omega_0 t + i k_{0z}} + c.c., \tag{1.10}$$

where $n_2 = 3\epsilon_0 Z_0 \chi^3/(2n_0)$ is called the Kerr nonlinear index. In the following the most important effects of the Kerr nonlinearity will be discussed: self focusing, self phase modulation, conical emission, and the formation of stable light filaments. Self focusing is a spatial effect of the Kerr nonlinearity, whereas self phase modulation is its temporal (longitudinal) effect.

### 1.2.1 First order propagation equation

The full wave equation is a vector wave equation which is second order in time and space and which is quite cumbersome to integrate numerically. As a result, it is very time-consuming to propagate this equation over relevant experimental distances. As a result, usually approximations are used to simplify the vector wave equation [11]. First, the coupling between polarization directions is neglected, which is weak as long the nonlinear refractive index $n_2/n \ll 1$ and as long as the laser beam is not focused tightly. Second it is assumed that the wave is evolving slowly $\partial_z F \ll k_0 F$ upon propagation (slowly evolving wave approximation). As a result the second derivative along the propagation direction $z$ can be neglected, resulting in a first-order differential equation, which effectively neglects the backward propagating wave obtained by the full second-order differential equation solution. The backward propagating part becomes important only when the refractive index changes rapidly in $z$ such as at an interface between air and a material. The resulting slowly

wave equation for the envelope $F$ of the forward propagating field then becomes

$$(\partial_z - \frac{n_0}{c}\partial_t - \frac{i}{2k_0}\nabla_\perp^2)F = \frac{\omega_0}{c}\frac{n_2 I_0}{2n_0}|F|^2 F, \tag{1.11}$$

where $\nabla_\perp^2 = \partial^2/\partial_x^2 + \partial^2/\partial_y^2$ is the transverse Laplacian operator. We have further assumed that the linear refractive index $n(\omega) = n(\omega_0)$ is frequency independent so that dispersion can be neglected. By using the transformation to a time variable moving with the pulse group velocity, $\tau = t - (n_0/c)z$, the time derivative in Eq.(1.11) can be eliminated and we obtain

$$(\partial_z - \frac{i}{2k_0}\nabla_\perp^2)F = I_0\frac{\omega_0}{c}\frac{n_n}{2n_0}|F|^2 F \tag{1.12}$$

with $F = F(\mathbf{x}, \tau)$ and $n_n = n_2 I_0$.

### 1.2.2 Self-Focusing

We will first apply Eq.(1.12) to the spatial effect of the Kerr nonlinearity which is self focusing. We focus on a short enough segment of the material so that diffraction, the second term on the left hand side of Eq.(1.12), may be neglected. Then Eq.(1.12) can be analytically integrated and one obtains the solution for $F$ as

$$F(\tau, r, z) = F_0(\tau, r)\exp(i\frac{\omega_0 n_n}{2cn_0}|F_0(\tau, r)|^2 z), \tag{1.13}$$

Where we have assumed that the transverse part of the envelope is radially symmetric ($r = \sqrt{x^2 + y^2}$) and the initial envelope is $F_0(\tau) = F(\tau, z = 0)$.

From Eq.(1.13) we find that the Kerr effect leads to a phase delay proportional to the pulse envelope $|F_0|^2$. The phase delay is the largest on the beam axis (where the optical intensity is highest) and smaller away from the axis. This is similar to the action of a lens: the wavefronts (of constant phase) are curved, so that the pulse is focused assuming a positive nonlinear index $n_2$, see Fig.(1.3). As the laser beam writes its own lens, the process is referred to as self focusing. Self focusing has important implications. In combination

with an aperture it is used as Kerr lens mode locking to generate ultrashort pulses in laser resonators [12]. Further, self focusing increases the laser peak intensity and therefore is of critical importance for the optical damage of materials and material machining [8]. Finally, for materials with negative $n_2$ the effect is reversed and results in self-defocusing, see Fig.(1.3)

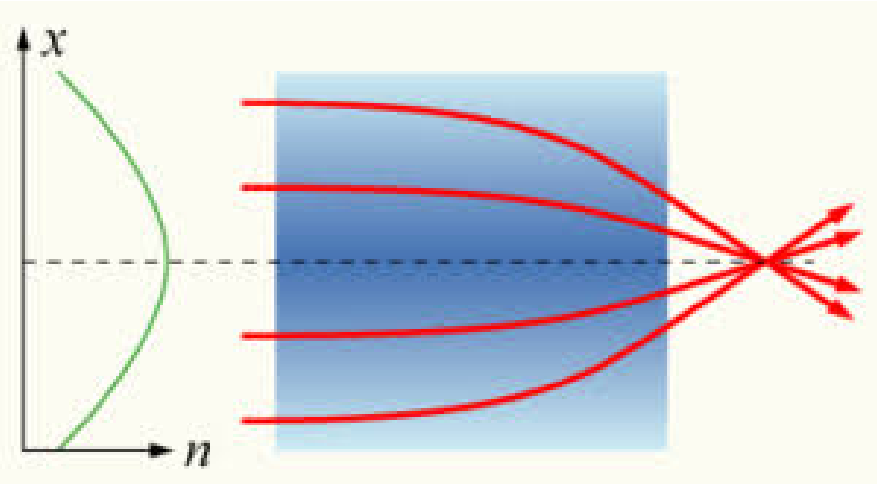


*Figure 1.3: The Kerr effect leads to a phase delay which is largest on the beam axis (where the optical intensity is highest) and smaller outside the axis. This is similar to the action of a lens: the wavefronts are deformed, so that the pulse is focused. Courtesy of Wikimedia Commons, photonicswiki.org*

### 1.2.3 Self phase modulation

In a similar way, the nonlinear index of a material also depends on time through the time dependence of the pulse envelope, where we assume $F = F_0(\tau)$ and here is constant with respect to transverse coordinates. From Eq. (1.13) we have $E = E_0 F_0(\tau) e^{-i\Phi(\tau)}$, where

$$\Phi(\tau) = \omega_0 \tau - \frac{\omega_0}{c} \bar{n}(\tau) z \tag{1.14}$$

with $\bar{n}(\tau) = \omega_0 n_n / (2cn_0)|F_0(\tau)|^2$. The time derivative of the phase, $d\Phi/d\tau = \omega(\tau)$ gives a time varying frequency

$$\omega(\tau) = \omega_0 - \frac{\omega_0}{c} \frac{d\bar{n}}{d\tau} z, \tag{1.15}$$

and the range of the frequency sweep is

$$\delta\omega(\tau) = \omega(\tau) - \omega_0 = -\frac{\omega_0}{c}\frac{d\bar{n}}{d\tau}z \tag{1.16}$$

From Eqs.(1.15) and (1.16) we see that the Kerr nonlinearity generates new frequencies in the pulse spectrum. From Figure (1.4) we find that red frequency components are generated at the leading edge of the pulse, whereas blue frequencies are added to the trailing edge of the laser pulse. The Kerr nonlinearity is the main process used for pulse shortening in ultrafast optics. From Fourier transform theory we would expect that a broader spectrum has to result in a shorter pulse. However, this is only true for transform limited (chirp free) pulses. As the new frequencies are not uniformly distributed throughout the pulse, but appear as a chirp, the pulse is not transform limited. In order to translate the new frequencies into a shorter pulse duration, the chirp has to be compensated which can be done by an element with negative group velocity dispersion, see Fig. (1.4).

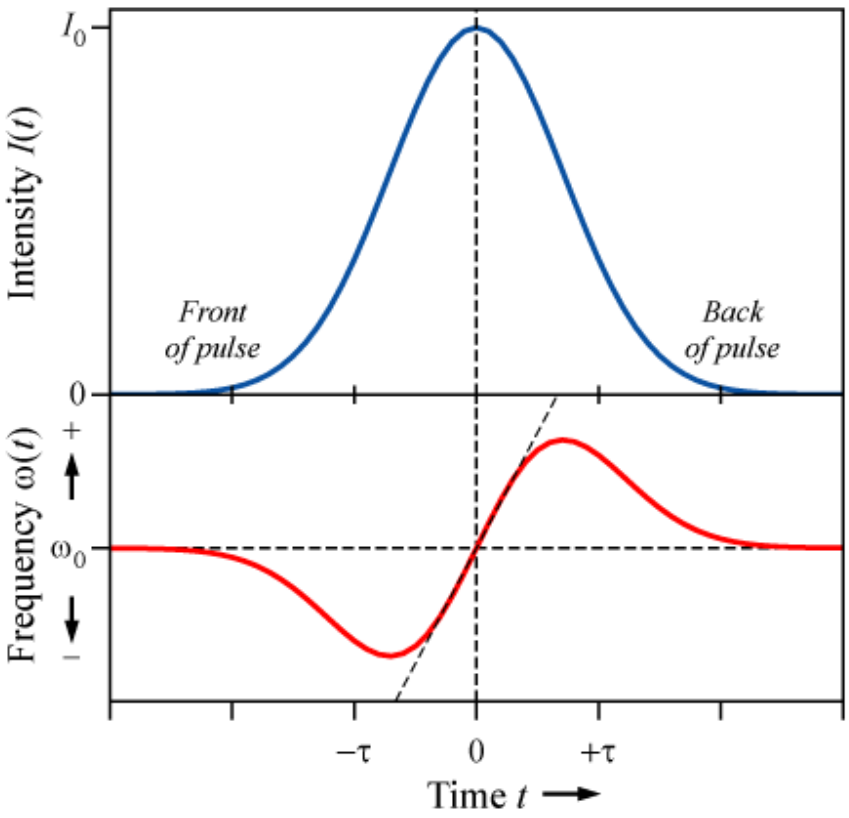


*Figure 1.4: Self phase moduation results in a broadening of the pulse spectrum. In the time domain this manifests as a frequency chirp, i.e. the frequency is changing over the pulse envelope. The front of the pulse shifts to higher frequencies, and the back of the pulse to lower frequencies. Following the dashed lines, we see that the centre of the pulse has an approximately linear frequency shift. By compensating for this frequency chirp in an optical element with negative group velocity dispersion, the spectral broadening is translated into temporal pulse shortening. (Courtesy of Wikimedia Commons, http://commons.wikimedia.org/)*

### 1.2.4 Filamentation and modulation instability

The Kerr nonlinearity can give rise to unstable behaviour. The detailed mathematics will be discussed in the main part of the thesis. Here, a more descriptive discussion is given. In one dimensional systems, such as fibers, the Kerr instability is referred to as modulation instability and leads to the temporal (longitudinal) breakup of long pulses or plane wave. Note that unstable behaviour can only occur in the presence of negative group velocity dispersion (GVD), sgn($\beta_2 = -1$, where $\beta_2$ is the GVD coefficient. Under this condition, a band of frequencies around the center frequency of the initial laser pulse expereinces gain; these frequencies grow out of noise and experience exponential amplification. When they become of the order of the intial pulse, they lead to a breakup of the pulse through intereference [13].

In three dimensions, the Kerr instability results in a breakup of the transverse part of the pulse which is refereed to as filamentation instability as it initializes the filamentation process. Note that this instability does not depend on the presence or the sign of group velocity dispersion. It appears for transverse off-axis components in a cone around the initial wavevector of the laser pulse. The band of generated frequencies is extremely wide and ranges from the ultraviolet to the mid-infrared wavelength regime [6]. This phenomenon triggers filamentation and the emission of the wide band of frequencies is known as conical emission. It has been observed in all kind of dielectric materials, from gases to liquids and solids. Although conical emission is involved in seeding the filamentation process, it keeps occuring once filamentation has happened.

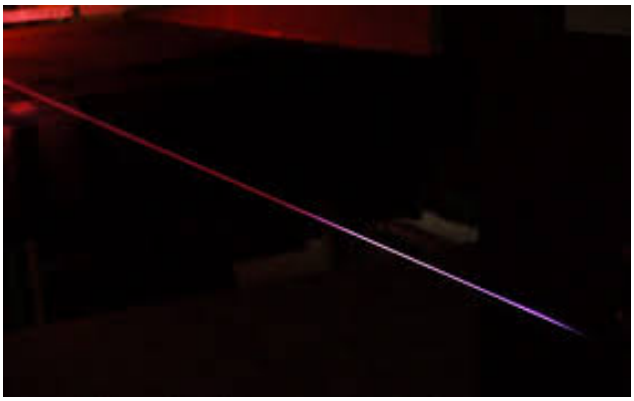

*Figure 1.5: The start of the filamentation arises from a minor disturbance of the laser beam propagating transversally. The filaments are extremely broadband in frequency as can be seen by the array of colours in this filament [14].*

Filamentation is the transverse breakup of a long initial pulse into one or several stable filaments that can propagate stably over long distances (kilometers in gases) without being affected by diffraction, see Fig.(1.5). As the intensity in the filament can become quite high, material damage can occur. Actually, evidence of filamentation was first noticed due to the traces of the filamentary damages found in glass [15]. Filamentation is of interest for a wide range of applications. Typical applications include remote sensing of atmospheric gases and aerosols, lightning and weather control, laser-induced spectroscopy, coherent anti-stokes Raman scattering, and the generation of sub-THz radiation. [16]. Finally, due to the long interaction distances of a filament, self-phase modulation is very effective and leads to extreme spectral broadening, which is known as white light generation, see Fig.(1.5). As a result, filaments are also used to generate ultrawide spectra and ultrashort pulses.

Filamentation is initiated by two processes, self-focusing and the Kerr instability. The exact interplay between these processes and the dynamics leading to filamentation is still not well understood. A major question is how a catastrophic collapse due to self-focusing is prevented [3]. Self-focusing increases the peak intensity which in turn enhances the self-focusing lens, so that in the absence of other processes the laser beam would be focused down to a point. This is referred to as catastrophic self-focusing. The most likely mechanism that can stabilize the self-focusing process is ionization [17].

Self-focusing increases the peak intensity, until it is strong enough to cause ionization. Ionization is strongest at the pulse peak where the highest density of free electrons is generated [18]. The resulting profile of free electrons acts as a negative lens that counteracts self-focusing and stabilizes the laser beam [19]. Before we go into this process in more detail, a brief review of optical field ionization will be given in the next section.

### 1.2.5 Optical field ionization

Photo ionization is a well known process, where a bound electron in a material (atom, molecule, solid) absorbs a single photon, is promoted to the continuum, and is set free. In the case of a solid the transition happens from the valence to the conduction band, where the electron can move freely, but it still bound within the solid [20].This process takes place at low intensities. What happens when the photon energy is not sufficient to bridge the energy between the bound state and the continuum?

In the under-resonant limit, where the photon energy is much smaller than the ionization energy $I_p$, optical field ionization takes place. This can only happen at high (non-perturbative) laser intensities. There are two processes, multi-photon ionization and tunnel ionization, see Fig.(1.6).

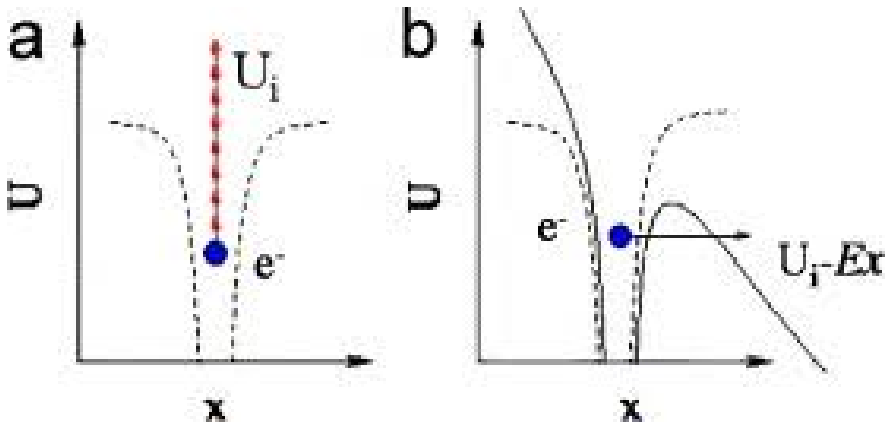


*Figure 1.6: (a) multiphoton and (b) tunnel ionization [3].*

Multi-photon ionization is dominant at somewhat lower intensties, whereas tunnel ionization dominates at the highest intensities. In multi-photon ionization the electron is promoted to the continuum by absorbing $n$ photons with $n\omega_0 > I_p$. In tunnel ionization, the electron tunnels through the barrier formed by the combined fields of confining potential and laser. The free electron is born outside the classical turning point, where it has energy greater than zero and where it can exist classically. Whereas multi-photon ionization happens continuously throughout the optical cycle, tunnel ionization occurs mainly around the peaks of the optical cycle where the field strength is highest [21].

### 1.2.6 Plasma Defocusing

The classical quiver motion $x + \Delta x$ of a free electron along the polarization direction of a laser field at $x$ is given by

$$m\frac{d^2\Delta x}{dt^2} = -eE(x,t), \tag{1.17}$$

where the space dependence of **E** is neglected, as the excursion amplitide of the electron in the laser field is much smaller than the laser wavelength. Further, we have assumed that the electric field is polarized along $x$-direction. Finally we assume a plane wave for the laser electric field, $E = E_0 \exp(i\omega_0 t)$. Then, integration of Eq.(1.19) yields [22]

$$\Delta x = \frac{e}{m\omega_0^2}E(x,t) \tag{1.18}$$

From that the polarization is determined by

$$P(x,t) = N(x,t)e\Delta x(t) = N(x,t)\frac{e^2}{m\omega_0^2}E(x,t), \tag{1.19}$$

where $N$ is the free electron density. Inserting $P$ in the wave equation (1.9) and obtain

$$\left(\frac{\partial^2}{\partial z^2} - \frac{1}{c^2}\frac{\partial}{\partial t}\right)E_0 e^{-i\omega_0 t + ik_p z} = -\frac{\omega_p^2}{c^2}\frac{\partial^2}{\partial t^2}E_0 e^{-i\omega_0 t + ik_p z}, \tag{1.20}$$

where

$$\omega_p^2 = \frac{Ne^2}{\epsilon_0 m} \tag{1.21}$$

is the plasma frequency.

The above equation is solved provided that

$$k_p = \frac{1}{c}\sqrt{\omega_0^2 - \omega_p^2}. \tag{1.22}$$

We can see from Eq.(1.22) that when the laser frequency is smaller than the plasma frequency, the wavevector turns imaginary, resulting in an evanescent wave that cannot propagate into the plasma, but is reflected [3].

In filamentation, ionization is usually weak enough so that $\omega_0 \gg \omega_p$ and $k_p \approx (1/c)(\omega_0 - \omega_p^2/(2\omega_0))$. As a result, the laser electric field can be written as

$$E(x,t) = E_0 \exp(-i\omega_0 t + ik_0 z - i\frac{N(x,t)e^2}{2\epsilon_0\omega_0 m}z). \tag{1.23}$$

Here, $k_0 = \omega_0/c$ and we have assumed that ionization creates a free electron profile $N(\mathbf{x},t)$ with maximum free electron density at the pulse peak. This term leads again to a phase curvature, such as in the case of self-focusing; however here the phase is lowered due to the opposite sign, so that the resulting phase curvature acts as a negative lens.

Filamentation dynamics is driven by the competing action of Kerr self-focusing and plasma self-

defocusing. This results in the modulation dynamics seen in Fig.(1.7), where first self-focusing dominates and then when the peak intensity has increased enough, plasma formation and self-defocuing takes over and widens the beam again. This can go back and forth for multiple times until the beam reaches equilibrium and a steady filament is formed [3].

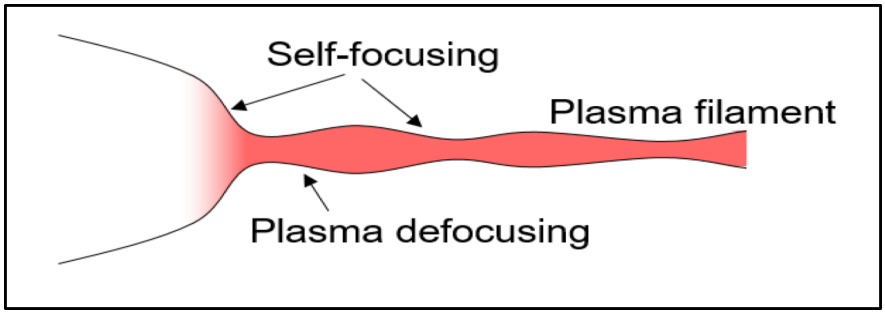


*Figure 1.7: The formation of a filament is driven by the competing actions of Kerr self-focusing and plasma self defocusing [3].*

.

### 1.2.7 Z-scan Method

So far we have derived and worked with the Kerr nonlinearity in the limit of perturbative nonlinear optics. Once the Kerr nonlinear index is known and for not too high laser intensities, pulse propagation in Kerr nonlinear media is well characterized.

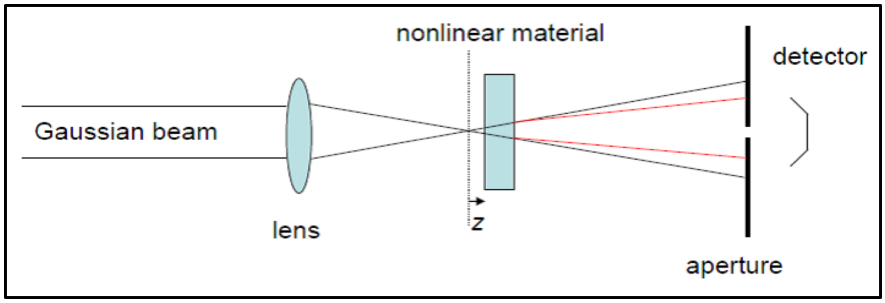


*Figure 1.8: Schematic of the Z-scan method for measurement of the Kerr nonlinear index, $n_2$ [23].*

Measurement of the Kerr nonlinear index is done by a standard method, termed the Z-scan method, see also the schematic in Fig.(1.8). A nonlinear material is placed in a Gaussian beam and shifted with regard to the focal plane of the Gaussian beam ($z = 0$). After the material there is an aperture followed by a detector, which measures the amount of transmitted light. We discuss here the case of positive $n_2$, which is depicted in

Fig.(1.9). When the nonlinear sample is moved ahead of the beam focus (negative z), the Kerr nonlinearity focuses the beam more strongly and moves the focal plane to negative$z$. The resulting larger distance to the aperture and the stronger diffraction result in less light going through the aperture and in a reduction of the transmitted signal. When the material is shifted to positive $z$ the opposite effect happens and the transmission increases [24].

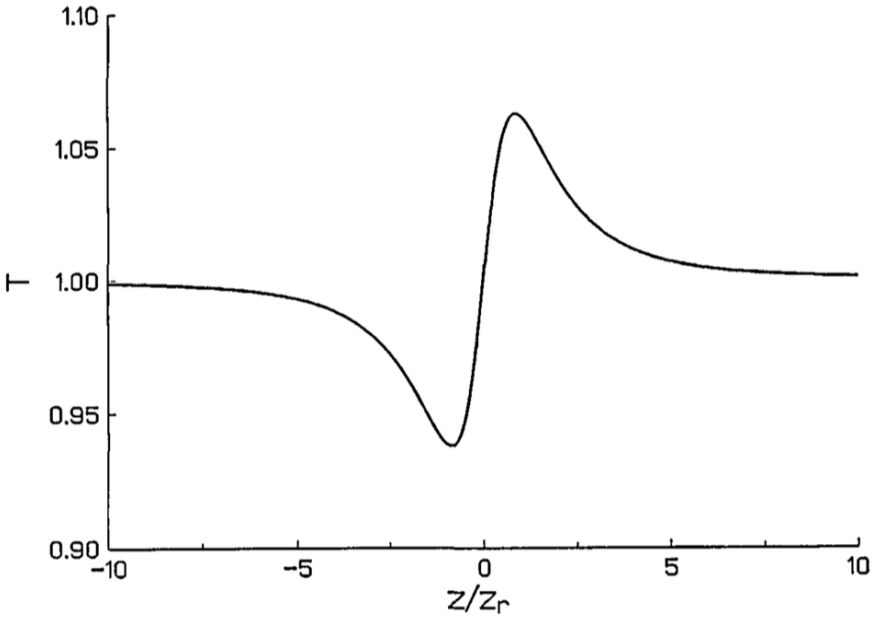


*Figure 1.9: When the $n_2$ positive will start the line a vally then peak, When the $n_2$ negative will the line start peak then a valley [25].*

### 1.2.8 Formulation of the research problem

So far we have shown that the Kerr nonlinear dyanmics in the limit of perturbative optics is well characterized, theoretically as well as experimentally. We have also found that during filamentation dynamics nonperturbative intensities are reached where ionization starts to occur. In this regime, very little is known about the functional form and magnitude of the Kerr nonlinearity. A change of the Kerr nonlinearity could have a substantial impact on filamentation dynamics and thus on the understanding of this highly nonlinear process.

The Z-scan method does not work at extreme intensities where ionization takes place, as it cannot

keep apart the positive and negative lens effect from the Kerr and plasma nonlinearity. To my knowledge at the moment no other method exists that is capable of measuring Kerr nonlinear processes at non-perturbative laser intensities.

We have discussed that during filamentation conical emission occurs. Only, recently it has been shown that a closely related process, Kerr Instability Amplification (KIA), can be utilized as a wideband infrared amplifier for ultrashort pulses. KIA was modelled based on a stability analysis of the scalar Kerr wave equation. Vectorial effects have not been considered so far.

The goal of my theoretical research is twofold, 1) understanding vectorial effects on KIA and 2) use the theory of KIA to discover new effects for measuring the Kerr nonlinearity in the limit of extreme, non-perturbative intensities.

In chapter 2 the vectorial theory of seeded KIA is developed. This work is novel and will be published as part of a book chapter [26]. In chapter 3, results obtained from the vector theory of KIA are discussed. In section , an introduction to KIA for plane seed waves is given, which also summarizes the results of the scalar stability analysis, see Ref. [7]. In section 3.2 the influence of vectorial effects on KIA are discussed. In general, they are found to be insignificant and do not affect KIA, as described by the scalar theory. Finally, in section 3.3 the theory of KIA is applied to devise novel ways to measure functional form and magnitude of the Kerr nonlinear coefficient.

# Chapter 2

# Seeded Kerr instability amplification

In this chapter I will devleop the theory of seeded Kerr instability amplification starting from Maxwell's equations and based on a linear stability analysis. The electric field is chosen as a superposition of a strong pump field and weak seed field. The nonlinearity is approximated by keeping only terms which are first order in the weak seed pulse.

## 2.1 Kerr instability vector wave equation

When a plane wave interacts with a Kerr nonlinear material, there exist a range of wavevectors and frequencies that experience exponential gain. The wavevectors lie on a cone around the pump plane wave and are responsible for the phenomenon of conical emission. On the other hand, they also cause breakup of the pump plane wave which is one of the mechanisms responsible for filamentation. It was recently shown that when the Kerr instability is seeded with a weak probe pulse it can be used as amplifier [27]. Kerr instability amplification has several favorable properties. It allows amplification of single cycle mid-infrared pulses to sub-mJ levels. The theory of Kerr instability amplification was developed using the scalar wave equation, i.e. coupling to other polarization directions was neglected.

In this chapter, I develop the full vector wave equation for seeded Kerr instability amplification. In the next chapter this theory is applied to develop concepts for measuring the Kerr nonlinearity. The electric field arising from the Kerr nonlinearity is treated in first order perturbation theory [28].

Our derivation starts from Maxwell's equations. In a Kerr nonlinear material, the polarization is given by

$$\mathbf{P} = \mathbf{P}^{(1)} + \mathbf{P}^{(3)} = \epsilon_0 \left[ \chi^{(1)}\mathbf{E} + \chi^{(3)}(\mathbf{E}\cdot\mathbf{E})\mathbf{E} \right]. \tag{2.1}$$

Where we assume $\chi^{(3)}$ to be a scalar quantity. The polarization is inserted into Maxwell's equations which consists of a set of four equations, the Ampere-Maxwell Law, Faraday's law, Gauss' law for electric fields, and Gauss' law for magnetic fields:

$$\boldsymbol{\nabla} \times \mathbf{E} = -\frac{\partial \mathbf{B}}{\partial t} \tag{2.2}$$

$$\boldsymbol{\nabla} \times \mathbf{H} = \mathbf{J} + \frac{\partial \mathbf{D}}{\partial t} \tag{2.3}$$

$$\boldsymbol{\nabla} \times \mathbf{D} = \rho \tag{2.4}$$

$$\boldsymbol{\nabla} \times \mathbf{B} = 0 \tag{2.5}$$

Here, $\mathbf{E}$ is the electric field, $\mathbf{D} = \epsilon_0\mathbf{E} + \mathbf{P}$ is the electric displacement field, $\mathbf{H} = \frac{1}{\mu_0}\mathbf{B}$ is the magnetic field, $\mathbf{B}$ is the magnetic flux density, $\mathbf{J} = 0$ is the free current density, and $\rho = 0$ is the free charge density. We assume here that no free charges exist. Further, $\mu_0$ and $\epsilon_0$ are the vacuum magnetic permeability and the electric permittivity, respectively. Next we use Eqs. (2.2) and (2.3) to eliminate the magnetic field. Further we use the vector identity

$$\nabla \times \nabla \times \mathbf{E}(r,t) = \nabla(\nabla \cdot \mathbf{E}(r,t)) - \nabla^2\mathbf{E}(r,t). \tag{2.6}$$

This yields a vector wave equation for the electric field,

$$\frac{\partial^2 \mathbf{E}}{\partial z^2} + \nabla_\perp^2 \mathbf{E} - \nabla(\nabla\cdot\mathbf{E}) - \frac{n^2{*}}{c^2}\frac{\partial^2 \mathbf{E}}{\partial t^2} = \mu_0 \frac{\partial^2}{\partial t^2}\mathbf{P}^{(3)}. \tag{2.7}$$

Here we have used the relations $c^2 = 1/(\epsilon_0\mu_0)$ and $n^2{*} = 1 + \chi^{(1)}$. The asterisk denotes convolution in time,

which is a linear response function. This arises from the fact that the linear refractive index is frequency-dependent and multiplies the Fourier-transformed electric field by the convolution theorem, it results in a linear response function $n^2*$ convolved with the time-dependent electric field. Moreover, we have divided the Laplacian operator into its longitudinal, $\partial_z^2$, and transverse, $\nabla_\perp^2$, components.

In order to solve Eq. (2.7) we use the following complex ansatz for the electric field

$$\mathbf{E} = \hat{\mathbf{x}} E_p e^{i\omega_p t - ik_p z} + \boldsymbol{\varepsilon}(x, y, z, t) \tag{2.8}$$

which consists of a main pump plane wave and of a perturbation field, $\boldsymbol{\varepsilon}$. The pump plane wave is polarized along $x$ and propagating along $z$ with peak electric field $E_p$, and center frequency $\omega_p$. The wavevector $k_p$ is defined below. The real component of electric field is given by $(\mathbf{E} + \mathbf{E}^*)/2$, where $^*$ denoted complex conjugation.

First, the polarization in Eq. (2.7) needs to be worked out. This is done by inserting the real electric field in $\mathbf{P}^{(3)}$ which gives

$$\mathbf{P}^{(3)} = \epsilon_0 \chi^{(3)} \left[ (\mathbf{E} \cdot \mathbf{E})\, \mathbf{E} + 2|\mathbf{E}|^2 \mathbf{E} + (\mathbf{E} \cdot \mathbf{E})\, \mathbf{E}^* + c.c. \right] \tag{2.9}$$

As discussed in the previous chapter, the general third order nonlinearity contains a contribution to third harmonic generation and a contribution to self phase modulation, i.e. the Kerr nonlinearity. We only keep the Kerr nonlinear contributions which are the second and the last term in Eq. (2.9), as the first term corresponds to third harmonic generation.

Inserting the ansatz (2.8) into Eq. (2.9) yields for the nonlinear polarization

$$\mathbf{P}^{(3)} = n_n \hat{\mathbf{x}} E_p e^{i(\omega_p t - k_p z)} + \frac{2n_n}{3} \left( \boldsymbol{\varepsilon} + 2\hat{\mathbf{x}} \varepsilon_x \right) + \frac{n_n}{3} \left( \boldsymbol{\varepsilon}^* + 2\hat{\mathbf{x}} \varepsilon_x \right) e^{2i(\omega_p t - k_p z)}, \tag{2.10}$$

where $\boldsymbol{\varepsilon} = (\varepsilon_x, \varepsilon_y, \varepsilon_z)$, and where we have kept only terms linear in the perturbation $\boldsymbol{\varepsilon}$. Here, we have used $n_n = n_2 I_p = 3\chi^{(3)} E_p^2$, where $I_p = n_p E_p^2/(2Z_0)$, where $n_p = n(\omega_p)$ and with $Z_0$ the vacuum impedance. As a

result the nonlinear Kerr coefficient $n_2 = 6Z_0\chi^{(3)}/n_p$. In most materials $n/n_n \ll 1$ which will be used here throughout the derivation.

Next we insert the ansatz (2.8) and the nonlinear polarization (2.10) into the wave equation (2.7). We take advantage of the fact that the plane wave is a formal solution of the vector wave equation $k_p = \omega_p/c(n_p+n_n)^{1/2}$. Here, $n_p = n(\omega_p)$ is the refractive index at the pump center frequency. However, the plane wave solution is not necessarily a stable solution. The resulting equation for the small perturbation $\boldsymbol{\varepsilon}$ tests the stability of the plane wave solution. It is

$$\left[\frac{\partial^2}{\partial z^2} + \nabla_\perp^2 - \nabla(\nabla\cdot) - \frac{n^2*}{c^2}\frac{\partial^2}{\partial t^2}\right]\boldsymbol{\varepsilon} = \frac{n_n}{3c^2}\frac{\partial^2}{\partial t^2}\left[2\boldsymbol{\varepsilon} + 4\hat{\mathbf{x}}\varepsilon_x + (\boldsymbol{\varepsilon}^* + 2\hat{\mathbf{x}}\varepsilon_x^*)\, e^{2i(\omega_p t - k_p z)}\right]. \tag{2.11}$$

To proceed further Eq. (2.13) is transformed into the Fourier domain by using the relation

$$\boldsymbol{\varepsilon}(\mathbf{x},t) = \left(\frac{1}{2\pi}\right)^{3/2}\int_{-\infty}^{\infty} d\omega dk_x dk_y \tilde{\boldsymbol{\varepsilon}}(\omega,k_x,k_y)\exp\left(ik_x x + ik_y y + i\omega t\right). \tag{2.12}$$

Together with the ansatz $\boldsymbol{\varepsilon} = \mathbf{u}\exp(i\omega_p t)$, the Fourier transformed perturbation is inserted into Eq. (2.7) which results in

$$\left[\frac{\partial^2}{\partial z^2} - k_\perp^2 - \hat{\mathbf{G}} + \frac{\omega^2}{c^2}\left(n^2 + 2n_n\right)\right]\tilde{\mathbf{u}} = -\frac{n_n\omega^2}{3c^2}\left[-4\hat{\mathbf{y}}\tilde{u}_y + \left(\tilde{\mathbf{u}}_{(-)}^* + 2\hat{\mathbf{x}}\tilde{u}_{x(-)}^*\right)e^{-2ik_p z}\right]. \tag{2.13}$$

Here, $\tilde{\mathbf{u}}(\Omega,\mathbf{k}_\perp,z)$ is the Fourier-transformed field, with $\Omega = \omega - \omega_p$, $\mathbf{k}_\perp = (k_x,k_y)$ and $k_\perp^2 = k_x^2 + k_y^2$. Note that $\tilde{\mathbf{u}}_{(-)}^* = \tilde{\mathbf{u}}^*(-\Omega,-\mathbf{k}_\perp,z)$. The minus sign comes from the fact that the Fourier transform of the complex

conjugate of a signal in time is the complex conjugate function of the negative frequency. Further,

$$\hat{\mathbf{G}} = \begin{bmatrix} -k_x^2 & -k_x k_y & ik_x\partial_z \\ -k_x k_y & -k_y^2 & ik_y\partial_z \\ ik_x\partial_z & ik_y\partial_z & \partial_z^2 \end{bmatrix} \tag{2.14}$$

is the Fourier transformed gradient of divergence operator.

This equation can be further simplified. We start with the $z$-component and define $k^2 = n^2\omega^2/c^2$, $k_n^2 = n_n\omega^2/c^2$, $k_v^2 = k^2 + 2k_n^2$, and $k_z^2 = k_v^2 - k_\perp^2$. Respectively, physically these are the linear wavenumber squared, the nonlinear wavenumber squared, the modified wavenumber of the perturbation squared, and the longitudinal component of the modified wavenumber of the perturbation squared. Further, we use $k_{v(-)} = k_v(-\Omega)$, $k_{z(-)} = k_z(-\Omega)$, and $k_{n(-)} = k_n(-\Omega)$. With these definitions Eq. (2.13) for the z-component becomes

$$\left\{k_z^2 k_{z(-)}^2 - ik_{z(-)}^2(k_x\partial_z u_x + k_y\partial_z u_y) - \frac{1}{9}k_n^2 k_{n(-)}^2\right\} u_z = \frac{i}{3}k_n^2 e^{-2ik_p z}\left(k_x\partial_z u_{x(-)}^* + k_y\partial_z u_{y(-)}^*\right) \tag{2.15}$$

By using $k_n^2/k_z^2 \ll 1$, which means that the nonlinear refractive index is very small compared to the linear index (which is valid for natural dielectric materials), Eq. (2.15) simplifies to

$$k_z^2 u_z = i\left(k_x\partial_z u_x + k_y\partial_z u_y\right) \tag{2.16}$$

With the help of Eq. (2.16), $u_z$ can be eliminated from Eq. (2.13) which yields

$$\left(1 + \frac{\partial_z^2}{k_z^2}\right)\left[\left(k_v^2 - k_y^2\right)u_x + k_x k_y u_y\right] = -k_n^2\left(u_{x(-)}^* e^{-2ik_p z}\right), \tag{2.17}$$

$$\left(1 + \frac{\partial_z^2}{k_z^2}\right)\left[\left(k_v^2 - k_x^2\right)u_y + k_x k_y u_x\right] = -\frac{1}{3}k_n^2\left[-4u_y + k_n^2 u_{y(-)}^* e^{-2ik_p z}\right]. \tag{2.18}$$

Eqs. (2.17) and (2.18) can be written as a 2x2 matrix equation for $\mathbf{u} = (u_x, u_y)$. Inversion of the 2x2 matrix on the LHS of the resulting equation gives

$$\left(k_z^2 + \partial_z^2\right)\mathbf{u} = -\frac{k_n^2}{k_v^2}\begin{bmatrix} k_v^2 - k_x^2 & -k_x k_y \\ -k_x k_y & k_v^2 - k_y^2 \end{bmatrix}\begin{pmatrix} u^*_{x(-)}e^{-2ik_p z} \\ -\frac{4}{3}u_y + \frac{1}{3}u^*_{y(-)}e^{-2ik_p z} \end{pmatrix}. \tag{2.19}$$

Finally we make the ansatz $\mathbf{u} = \mathbf{v}\exp(-ik_p z)$ to eliminate the exponential terms on the right-hand-side of Eq. (2.19). This results in

$$\left(k_z^2 + (\partial_z - ik_p)^2\right)\mathbf{v} = -\frac{k_n^2}{k_v^2}\hat{M}\mathbf{v}^*_{(-)}, \tag{2.20}$$

where

$$\hat{M} = \begin{bmatrix} k_v^2 - k_x^2 & -\frac{1}{3}k_x k_y \\ -k_x k_y & \frac{1}{3}(k_v^2 - k_y^2) \end{bmatrix} \tag{2.21}$$

Here we have used the fact that unstable behavior occurs to leading order as a result of coupling between $\mathbf{v}$ and $\mathbf{v}^*$ and that $k_n^2 \ll k_v^2$. As a result, the term $4k_n^2/(3k_v^2)v_y$ can be neglected. Further the different prefactors of $v^*_{x(-)}$ and $(1/3)v^*_{y(-)}$ on the right-hand-side of Eq.(2.19) have been pulled into $\hat{M}$.

Equation (2.20) is the vector equation of motion governing the evolution of the Kerr nonlinear instability. They generalize previous work [7] from scalar to vector theory. To reduce to scalar theory, we take $\hat{M} \to k_v^2$ and $\boldsymbol{v} \to v_x$ in Eq. (2.20).

## 2.2 Decoupling the Kerr instability vector wave equation

For the solution of Eq. (2.20) we need the equation of motion of $\mathbf{v}^*_{(-)}$. This is obtained by taking the complex conjugate of Eq. (2.20) and changing in all functions $\Omega \to -\Omega$. As a result we obtain

$$\left(k^2_{z(-)} + (\partial_z + ik_p)^2\right)\mathbf{v}^*_{(-)} = -\frac{k^2_{n(-)}}{k^2_{v(-)}}\hat{M}_{(-)}\mathbf{v}, \tag{2.22}$$

Next, Eq. (2.20) is multiplied by $\left(k^2_{z(-)} + (\partial_z + ik_p)^2\right)$ and the resulting right-hand-side is replaced by using Eq. (2.22) which eliminates $\mathbf{v}^*_{(-)}$. The resulting equation for $\mathbf{v}$ is

$$\left(k^2_z + (\partial_z - ik_p)^2\right)\left(k^2_{z(-)} + (\partial_z + ik_p)^2\right)\mathbf{v} = -\frac{k^2_n k^2_{n(-)}}{k^2_v k^2_{v(-)}}\hat{M}\hat{M}_{(-)}\mathbf{v}, \tag{2.23}$$

where $\hat{M}_{(-)} = \hat{M}(-\Omega, -k_x, -k_y)$. The matrix $\hat{L} = \hat{M}\hat{M}_{(-)}$ is given by

$$\hat{L} = \begin{bmatrix} l_{11} & l_{12} \\ l_{21} & l_{22} \end{bmatrix} = \begin{bmatrix} k^2_v k^2_{v(-)} - k^2_x\left(k^2_v + k^2_{v(-)} - k^2_x - \frac{1}{3}k^2_y\right) & -\frac{1}{3}k_x k_y\left(\frac{1}{3}k^2_{v(-)} + k^2_v - k^2_x - \frac{1}{3}k^2_y\right) \\ -k_x k_y\left(\frac{1}{3}k^2_v + k^2_{v(-)} - k^2_x - \frac{1}{3}k^2_y\right) & \frac{1}{9}\left[k^2_v k^2_{v(-)} - k^2_y\left(k^2_v + k^2_{v(-)} - 3k^2_x - k^2_y\right)\right] \end{bmatrix} \tag{2.24}$$

As $\hat{L}$ does not depend on $z$, Eq. (2.23) can be solved by diagonalizing $\hat{L}$. This is done by choosing the ansatz $\mathbf{v} = \hat{U}\mathbf{w}$, where $\hat{U}$ is a unitary matrix that diagonalizes $\hat{L}$, $\hat{D} = \hat{U}^{-1}\hat{L}\hat{U}$ with the eigenvalues, $\lambda_x \neq 0$ and $\lambda_y \neq 0$. The solution of the resulting equation

$$\left(k^2_z + (\partial_z - ik_p)^2\right)\left(k^2_{z(-)} + (\partial_z + ik_p)^2\right)\mathbf{w} = -\frac{k^2_n k^2_{n(-)}}{k^2_v k^2_{v(-)}}\hat{D}\mathbf{w}, \tag{2.25}$$

are the plane waves

$$\mathbf{w}(z) = \exp\left(i\mathbf{K}z\right)\mathbf{w}(z=0) \tag{2.26}$$

with $\mathbf{K} = (K_x, K_y)$ to be determined in the next section. Here, $\mathbf{w}(z=0) = \hat{U}^{-1}\mathbf{v}(z=0)$ represents the initial condition. Combining these results yields the solution of Eq. (2.23) as

$$\mathbf{v}(z) = \hat{U}\exp(i\hat{K}z)\hat{U}^{-1}\mathbf{v}(z=0) = \hat{P}(z)\mathbf{v}(z=0), \tag{2.27}$$

where $\hat{P}(z)$ is the evolution matrix that propagates $\mathbf{v}$ from $z=0$ to $z$.

The unitary transformation matrix $\hat{U}$ and the diagonal matrix $\hat{K}$ are calculated to order $O(l_{12}l_{21})$ which is consistent with terminating the calculation at powers $k_x^4$, $k_y^4$, $k_x^2k_y^2$, as $k_{x,y}^2/k_v^2 \ll 1$. The resulting diagonal matrix

$$\hat{D} = \begin{bmatrix} \lambda_x & 0 \\ 0 & \lambda_y \end{bmatrix} = \begin{bmatrix} l_{11} + \frac{l_{12}l_{21}}{l_{11}-l_{22}} & 0 \\ 0 & l_{22} - \frac{l_{12}l_{21}}{l_{11}-l_{22}} \end{bmatrix} \tag{2.28}$$

By approximating $l_{11} - l_{22} \approx (8/9)k_v^2k_{v(-)}^2$ we obtain for

$$\frac{l_{12}l_{21}}{l_{11}-l_{22}} \approx \frac{3}{8}\frac{k_x^2k_y^2}{k_v^2k_{v(-)}^2}(k_v^2 + \frac{1}{3}k_{v(-)}^2)(\frac{1}{3}k_v^2 + k_{v(-)}^2). \tag{2.29}$$

The diagonalization matrix is found to be

$$\hat{U} = \frac{1}{l_{11}-l_{22}}\begin{bmatrix} l_{11}-l_{22} & -l_{12} \\ l_{21} & l_{11}-l_{22} \end{bmatrix}, \tag{2.30}$$

and its inverse is

$$\hat{U}^{-1} = \frac{1}{l_{11}-l_{22}}\begin{bmatrix} l_{11}-l_{22} & l_{12} \\ -l_{21} & l_{11}-l_{22} \end{bmatrix}. \tag{2.31}$$

With knowledge of $\hat{K}$, $\hat{U}$, and $\hat{U}^{-1}$ the propagator $\hat{P}$ is found to be

$$\hat{P}(z) = \begin{bmatrix} e^{iK_x z} + \frac{l_{12}l_{21}}{(l_{11}-l_{22})^2} e^{iK_y z} & \frac{l_{12}}{(l_{11}-l_{22})} \left(e^{iK_x} - e^{iK_y z}\right) \\ \frac{l_{21}}{(l_{11}-l_{22})} \left(e^{iK_x} - e^{iK_y z}\right) & e^{iK_y z} + \frac{l_{12}l_{21}}{(l_{11}-l_{22})^2} e^{iK_x z} \end{bmatrix}. \tag{2.32}$$

From Eqs. (2.28) and (2.24) we see that $K_x \approx 9K_y$. As a result, $K_x$ will give the dominant contribution to unstable growth and the terms containing $K_y$ can be neglected. Consequently, the propagator simplifies to

$$\hat{P}(z) = \begin{bmatrix} 1 & \frac{l_{12}}{(l_{11}-l_{22})} \\ \frac{l_{21}}{(l_{11}-l_{22})} & \frac{l_{12}l_{21}}{(l_{11}-l_{22})^2} \end{bmatrix} e^{iK_x z}. \tag{2.33}$$

By inserting the coefficients in Eq. (2.33) we finally obtain

$$\hat{P}(z) = \begin{bmatrix} 1 & -\frac{3}{8}\frac{k_x k_y}{k_v^2 k_{v(-)}^2} \left(\frac{1}{3}k_{v(-)}^2 + k_v^2 - k_x^2 - \frac{1}{3}k_y^2\right) \\ -\frac{9}{8}\frac{k_x k_y}{k_v^2 k_{v(-)}^2} \left(\frac{1}{3}k_v^2 + k_{v(-)}^2 - k_x^2 - \frac{1}{3}k_y^2\right) & \frac{27}{64}\frac{k_x^2 k_y^2}{k_v^4 k_{v(-)}^4}(k_v^2 + \frac{1}{3}k_{v(-)}^2)(\frac{1}{3}k_v^2 + k_{v(-)}^2) \end{bmatrix} e^{iK_x z}. \tag{2.34}$$

This result generalizes Kerr instability analysis from scalar [7] to vector theory. What remains to be done for a complete solution is determination of the wavevector $\mathbf{K} = (K_x, K_y)$ of the plane wave solution (2.26) of Eq.(2.25). This will be done in the next section.

## 2.3 Determination of the complex wavevector of the vector Kerr instability

In order to make further progress in solving the the vector wave equation (2.25) and thus, in determining $K_x$ and $K_y$, the sign swapped functions need to be specified. To this end, they need to be split in even/odd parts that are symmetric/antisymmetric with regard to sign change. We start with $k(\omega)$ and introduce $n_p = n(\omega_p)$ The refractive index can be recast into $n(\omega) = n_p + \Delta n(\Omega)$, where $\Delta n(\Omega) = n_g(\Omega) + n_u(\Omega)$ is split into even

and odd parts, $n_{g,u} = \frac{1}{2}[\Delta n(\Omega) \pm \Delta n(-\Omega)]$, so that $n_g(-\Omega) = n_g(\Omega)$ and $n_u(-\Omega) = -n_u(\Omega)$. Inserting these definitions we obtain $k_v = k_v(\omega_p) + D_g + D_u$, where

$$D_g(\Omega) = \frac{n_g(\Omega)\omega_p + n_u(\Omega)\Omega}{c}, \tag{2.35a}$$

$$D_u(\Omega) = \frac{(n_p + n_g(\Omega))\Omega + n_u(\Omega)\omega_p}{c}. \tag{2.35b}$$

Using the above definitions, the sign flipped wavevector is given by $k_{v(-)} = k_v(\omega_p) + D_g - D_u$. The terms $D_{g,u}$ are the linear even and odd dispersion terms. For $\Omega/\omega_p \ll 1$, $n_u \approx n_p'\Omega$ and $n_g \approx n_p''\Omega^2/2$. To illustrate the lowest order of our general dispersive functions, we obtain from Eq. (2.35) $D_g \approx (\beta_2/2)\Omega^2$ and $D_u \approx \beta_1\Omega$ with $\beta_1 = [dk/d\omega](\omega_p) = (n_p + n_p'\omega_p)/c$ group velocity and $\beta_2 = [d^2k/d\omega^2](\omega_p) = (n_p''\omega_p + 2n_p')/c$ group velocity dispersion; prime and double prime denote first and second frequency derivative, respectively. We assume $n_n$ constant, which is a reasonable approximation for frequencies much smaller than the material bandgap. This makes the sign flip operation for the nonlinear wavevector trivial, $k_{n(-)}^2 = n_n(\omega_p - \Omega)^2/c^2$.

Armed with the knowledge of the sign swapped functions, we can determine $K_x$ and $K_y$; the Ansatz (2.26) is inserted into the vector wave equation (2.25) resulting in an algebraic fourth order equation. On the right-hand-side of Eq. (2.25) we find terms $\propto k_n^2 k_{n(-)}^2 \lambda_x/(k_v^2 k_{v(-)}^2)$ and $\propto k_n^2 k_{n(-)}^2 \lambda_y/(k_v^2 k_{v(-)}^2)$ for the $K_x$- and $K_y$- equations, respectively. As $\lambda_x/\lambda_y \approx 9$, the equation for $K_x$ determines the dominant unstable growth; as a result, the second equation for $K_y$ is neglected and we focus on the $K_x$ equation,

$$\begin{aligned}&\left[(K_x^2 - D_u^2\sigma^2) + (D_u^2 - k_p^2)(\sigma^2 - 1) + k_\perp^2\right]^2 - \\ &-4k_p^2\left(K_x + D_u\sigma\right)^2 - k_n^2 k_{n(-)}^2\left(1 + r(k_x, k_y)\right) = 0\end{aligned} \tag{2.36}$$

with $\sigma(\Omega) = \left(k_v(\omega_p) + D_g\right)/k_p$, from which we obtain the approximate expression $\sigma^2 - 1 \approx 2D_\mathrm{g}/k_\mathrm{p}$ for later use. Further, we have introduced $\lambda_x/(k_v^2 k_{v(-)}^2) = 1 + r(k_x, k_y)$ with

$$r = -\frac{k_x^2}{k_v^2 k_{v(-)}^2}\left(k_v^2 + k_{v(-)}^2 - k_x^2 - \frac{1}{3}k_y^2\right) + \frac{3}{8}\frac{k_x^2 k_y^2}{k_v^4 k_{v(-)}^4}(k_v^2 + \frac{1}{3}k_{v(-)}^2)(\frac{1}{3}k_v^2 + k_{v(-)}^2) \tag{2.37}$$

The dominant part of the solution is given by the the second term of Eq. (2.36), which gives $K_x \approx -D_u\sigma$. As a result, we can approximate in the first term of Eq. (2.36), $K_x^2 - (D_u\sigma)^2 \approx -2D_u\sigma(K_x + D_u\sigma)$. This amounts to neglecting backward propagating solutions and results in a reduction to a quadratic equation,

$$\begin{aligned} &4(K_x + \sigma D_u)^2\left(k_p^2 - (\sigma D_u)^2\right) - 4(K_x + \sigma D_u)\times \\ &\times \sigma D_u\left(\kappa_\perp^2 - k_\perp^2\right) - \left(\kappa_\perp^2 - k_\perp^2\right)^2 + \left(k_n k_{n(-)}(1+r)\right)^2 = 0. \end{aligned} \tag{2.38}$$

Here, $\kappa_\perp^2(\Omega) = (k_p^2 - D_u^2)(\sigma^2 - 1)$. Solution of Eq. (2.38) yields $K_x = K_u(\Omega) + K_g(\Omega)$ with

$$K_u(\mathbf{k}_\perp, \Omega) = -\sigma D_u\left[1 - \frac{1}{2}\frac{\kappa_\perp^2 - k_\perp^2}{k_p^2 - (\sigma D_u)^2}\right] \tag{2.39a}$$

$$K_g(\mathbf{k}_\perp, \Omega) = -\frac{1}{2}\frac{k_p\sqrt{\left(\kappa_\perp^2 - k_\perp^2\right)^2 - \delta_\perp^4(1+r)^2}}{k_p^2 - (\sigma D_u)^2} \tag{2.39b}$$

and

$$\delta_\perp^2(\Omega) = \frac{k_n k_{n(-)}}{k_p}\sqrt{k_p^2 - (\sigma D_u)^2}. \tag{2.40}$$

Physically, $K_u$ is the wavevector of the perturbation, which couples transverse coordinates and odd dispersive terms of all order. To first order, $K_u \approx D_u \approx \beta_1\Omega$, which is the group velocity term of the usual linear wavevector, $k$. Further, $K_g$ is the wavevector of the perturbation which couples transverse coordinates and even dispersive terms of all order, and may become imaginary, resulting in instability. Also, $\delta_\perp^2$ denotes the transverse half-width squared over which the instability exists, which is a function of frequency. In the appropriate limits, Eq.(2.39b) goes over into the temporal modulation instability [30]−neglect transverse coordinates and consider small detuning, $\Omega$, and the spatial filamentation instability [31] −consider zero detuning, $\Omega = 0$. Note that the quadratic equation corresponds to a second order Mathieu-type differential equation that supports unstable solutions. When the argument of the square root in $K_g$ is negative, exponential growth happens with intensity gain $g = -2\mathrm{Im}(K_g)$. In the limit of $k_p^2 = (\sigma D_u)^2$, which occurs for $\Omega \approx \pm\omega_p$, the quadratic equation (2.38) reduces to a linear equation and $K$ becomes real; this has to be treated separately.

## 2.4 Summary of results

In this chapter we have derived a solution for the vector Kerr instability. In the following the results are summarized. A small perturbation $\mathbf{v}(z=0)$ develops as

$$\mathbf{v}(z) = \hat{P}(z)\mathbf{v}(z=0), \tag{2.41}$$

where the progagator matrix is given by

$$\hat{P}(z) = \begin{bmatrix} 1 & -\frac{3}{8}\frac{k_x k_y}{k_v^2 k_{v(-)}^2}\left(\frac{1}{3}k_{v(-)}^2 + k_v^2 - k_x^2 - \frac{1}{3}k_y^2\right) \\ -\frac{9}{8}\frac{k_x k_y}{k_v^2 k_{v(-)}^2}\left(\frac{1}{3}k_v^2 + k_{v(-)}^2 - k_x^2 - \frac{1}{3}k_y^2\right) & \frac{27}{64}\frac{k_x^2 k_y^2}{k_v^4 k_{v(-)}^4}(k_v^2 + \frac{1}{3}k_{v(-)}^2)(\frac{1}{3}k_v^2 + k_{v(-)}^2) \end{bmatrix} e^{iK_x z}. \tag{2.42}$$

The perturbation evolves as determined by the wavevector of the Kerr instability $K_x = K_u(\Omega) + K_g(\Omega)$ with

$$K_u(\mathbf{k}_\perp, \Omega) = -\sigma D_u \left[1 - \frac{1}{2}\frac{\kappa_\perp^2 - k_\perp^2}{k_p^2 - (\sigma D_u)^2}\right] \tag{2.43a}$$

$$K_g(\mathbf{k}_\perp, \Omega) = -\frac{1}{2}\frac{k_p\sqrt{\left(\kappa_\perp^2 - k_\perp^2\right)^2 - \delta_\perp^4(1+r)^2}}{k_p^2 - (\sigma D_u)^2}, \tag{2.43b}$$

with

$$\kappa_\perp^2(\Omega) = (k_p^2 - D_u^2)(\sigma^2 - 1), \tag{2.44}$$

where physically, $\kappa_\perp$ is the frequency-dependent wavevector that maximizes the instability. As it is non-zero, it demonstrates that non-collinear angles (which change with frequency) between pump and seed result in optimal amplification.

$$\delta_\perp^2(\Omega) = \frac{k_n k_{n(-)}}{k_p}\sqrt{k_p^2 - (\sigma D_u)^2}, \tag{2.45}$$

and

$$r = -\frac{k_x^2}{k_v^2 k_{v(-)}^2}\left(k_v^2 + k_{v(-)}^2 - k_x^2 - \frac{1}{3}k_y^2\right) + \frac{3}{8}\frac{k_x^2 k_y^2}{k_v^4 k_{v(-)}^4}(k_v^2 + \frac{1}{3}k_{v(-)}^2)(\frac{1}{3}k_v^2 + k_{v(-)}^2). \tag{2.46}$$

When the argument of the square root in $K_g$ is negative, exponential growth happens with intensity gain $g = -2\mathrm{Im}(K_g)$.

The difference between scalar theory published previously [7] and the current vector theory comes from the factor $r$ and from the propagator $P$ coupling $x$- and $y$- polarization. In the scalar limit, we set $r = 0$ and all results are radially symmetric, i.e. depend only on $k_\perp$; for each frequency $\Omega$ the gain $g$ is maximum at transverse wavevector

$$\bar{k}_\perp(\Omega) = \begin{cases} \kappa_\perp & \text{for } \kappa_\perp^2 \geq 0 \\ 0 & \text{for } \kappa_\perp^2 < 0 \end{cases} \tag{2.47}$$

and is denoted by $\bar{g} = g(k_\perp = \bar{k}_\perp(\Omega), \Omega)$ with

$$\bar{g}(\Omega) = \begin{cases} \frac{k_p\sqrt{\delta_\perp^4 - \left(\kappa_\perp^2 - \bar{k}_\perp^2\right)^2}}{k_p^2 - (\sigma D_u)^2} & \text{elsewhere} \\ 0 & \text{for } \kappa_\perp^2 < 0, \kappa_\perp^4 > \delta_\perp^4; \end{cases} \tag{2.48}$$

Note that $\kappa_\perp^2 \propto \sigma^2 - 1 \approx (2/n_p)(n_g + n_u\Omega/\omega_p)$. Depending on the material and $\omega_p$, the two terms $n_g$ and $n_u\Omega/\omega_p$ can have opposite or equal signs. As $g(k_\perp^2 = \bar{k}_\perp^2 \pm \delta_\perp^2) = 0$, the transverse wavevector halfwidth squared over which KIA gain occurs for a given $\Omega$ is given by $\delta_\perp^2(\Omega)$. The relation $k_\perp^2 = \bar{k}_\perp^2 \pm \delta_\perp^2$ defines curves in the $k_\perp - \Omega$ plane at which gain disappears. The curve defined by the expression with the minus sign exists only for $\kappa_\perp^2 \geq \delta_\perp^2$.

Vectorial effects are negligible as long as to leading order $r_0 \ll 1$ with

$$r_0 = \frac{k_x^2\left(k_v^2 + k_{v(-)}^2\right)}{k_v^2 k_{v(-)}^2}. \tag{2.49}$$

When this term becomes appreciable it breaks the radial symmetry of Kerr instability growth. For a given $K_x$ maximum gain is still achieved at $\bar{k}_\perp(\Omega) = \kappa_\perp$, however the maximum gain becomes $K_x$ dependent

$$\bar{g}(\Omega, k_x) = \frac{k_p \delta_\perp^2 \left[1 - r_0(k_x)\right]}{k_p^2 - (\sigma D_u)^2} \tag{2.50}$$

which breaks the radial symmetry.

# Chapter 3

# Seeded Kerr instability amplification

In the following, the results for plane wave KIA are derived in general. Then, two example materials will be quantitatively analyzed. In section (3.2), scalar theory ($r_0 = 0$) is shown to be justified, which simplifies the analysis without losing important physics.

## 3.1 Seeded Kerr instability amplification of plane waves

A seed plane wave

$$\tilde{v}_x(z=0) = (2\pi)^{3/2} E_s \delta(k_x - \bar{k}_{\perp s})\delta(k_y)\delta(\Omega - \Omega_s) \tag{3.1}$$

experiences maximum gain according to the relations given in section 2.4, namely Eqs.(2.43)−(2.50), assuming $r \approx r_0 = 0$. Here, $\bar{k}_{\perp s} = \bar{k}_\perp(\Omega_s)$. After material length $l$ the electric field is determined by the inverse Fourier transform of $\tilde{v}_x(0)\exp(iK_v l)$ which yields

$$\varepsilon_x(\mathbf{x}, t) = E_s \exp\left(\frac{1}{2}\bar{g}(\Omega_s)l - i\mathbf{K}_s\mathbf{x} + i\omega_s t\right). \tag{3.2}$$

Here, $\mathbf{K}_s = \mathbf{K}(\Omega_s) = (\bar{k}_{\perp s}, 0, K_{zs})$ is the seed wavevector, $K_{zs} = K_z(\Omega_s) = k_p + [\sigma D_u](\Omega_s)$, $\mathbf{x} = (x, y, z = l)$, $\omega_s = \omega_p + \Omega_s$, and $E_s$ is the seed electric field strength. We find that optimum amplification takes place when the seed propagation axis lies on a cone around the pump wavevector with half-angle

$$\theta_s = \theta(\Omega_s) = \arctan\left(\bar{k}_{\perp s}/K_{zs}\right). \tag{3.3}$$

Note that $\theta_s$ is related to but not necessarily the same as the conical emission angle. Conical emission grows out of noise and operates in the regime where filamentation has drastically modified the pump pulse. Seeded amplification happens over distances long before filamentation sets in.

Now, we will quantitatively analyze plane wave Kerr instability amplification (KIA) in two example dielectric solids, $CaF_2$ and KBr. We chose two different pump wavelengths $\lambda_p = 0.85,\ 2.1\,\mu$m. The $CaF_2$ and KBr crystals have transmission windows of $0.3 - 8\,\mu$m and $0.25 - 25\,\mu$m, respectively [32]. In all figures, the linear (by means of Sellmeier formulae) and nonlinear indices for $CaF_2$ are given by Malitson [33], and $n_2 = 2 \times 10^{-16}$ cm$^2$/W [34], respectively. The linear and nonlinear indices for KBr are given by Li [35], and $n_2 = 6 \times 10^{-16}$ cm$^2$/W [36], respectively. Finally, the peak pump intensities used are $I_p = 50$ TW/cm$^2$ and $I_p = 8$ TW/cm$^2$ for $CaF_2$ and KBr, respectively. Note that these intensities are chosen carefully and are valid for the damage threshold of each material in question, see Nesrallah and Brabec [7] for more detail.

In Fig. 3.1(a) the intensity gain profile, $g = 2\mathrm{Im}(K_g)$, is plotted versus $\omega_s/\omega_p$ and $k_\perp/k_p$. The solid white line represents $\bar{k}_\perp$. The pump wavelength is $\lambda_p = 2\pi c/\omega_p = 0.85\,\mu$m and pump intensity is $I_p = 50$ TW/cm$^2$. Amplification occurs over a wide spectral range from $0.45 - 15\,\mu$m. The gain ceases along two curves which are defined by the relation discussed above Eq. (3.6). In Fig. 3.1(b) the maximum gain $\bar{g}$ is shown on the infrared side versus seed frequency $\nu_s$ (bottom axis) and seed wavelength $\lambda_s$ (top axis). The two pump wavelengths $\lambda_p = 0.85, 2.1\,\mu$m correspond to the solid blue and dashed green curves, respectively, in 3.1(b) and (c). Maximum gain reaches a global maximum when pump and seed frequency are equal, and decreases with longer wavelengths. Note that energy is conserved regardless of the detuning $\Omega$ since we have $2\omega_p = (\omega_p + \Omega) + (\omega_p - \Omega)$, where 2 pump photons are equal to the signal, $(\omega_p + \Omega)$ and idler $(\omega_p - \Omega)$ photons. The idler is equivalent to the complex conjugate of the signal (seed). As well, momentum is conserved as

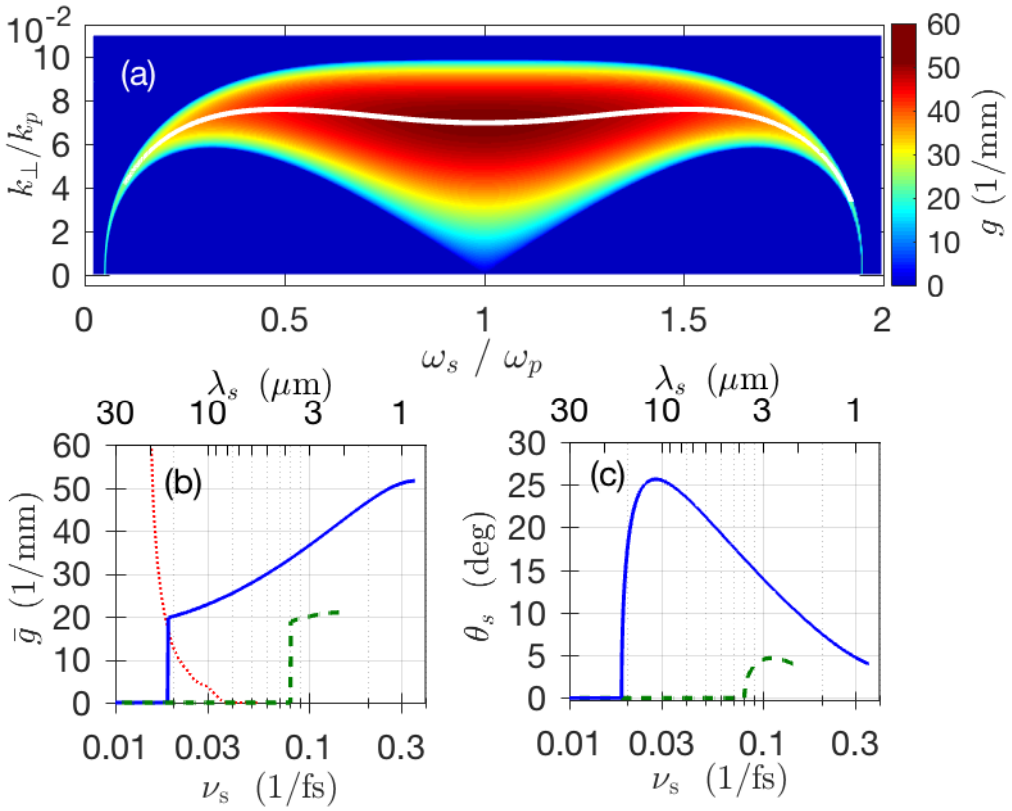


*Figure 3.1: Plane wave amplification in $CaF_2$ crystal. (a) Kerr instability gain, $g$ versus $\omega_s/\omega_p$ and $k_\perp/k_p$ (transverse over pump wavevector); pump wavelength $\lambda_p = 0.85\,\mu m$. The white line indicates $\bar{k}_\perp$ at which maximum gain $\bar{g} = g(\bar{k}_\perp)$ occurs, see Eq. (2.50). (b) $\bar{g}$ versus seed frequency $\nu_s = \omega_s/(2\pi)$ (bottom) and seed wavelength $\lambda_s$ (top); red dotted line represents absorption. (b)-(c) $\lambda_p = 0.85,\ 2.1\,\mu m$ corresponds to blue full, green dashed curves, respectively. (c) Angle of inclination between pump and seed beam $\theta_s$ at which maximum amplification takes place versus $\nu_s$ and $\lambda_s$, see Eq. (3.3).*

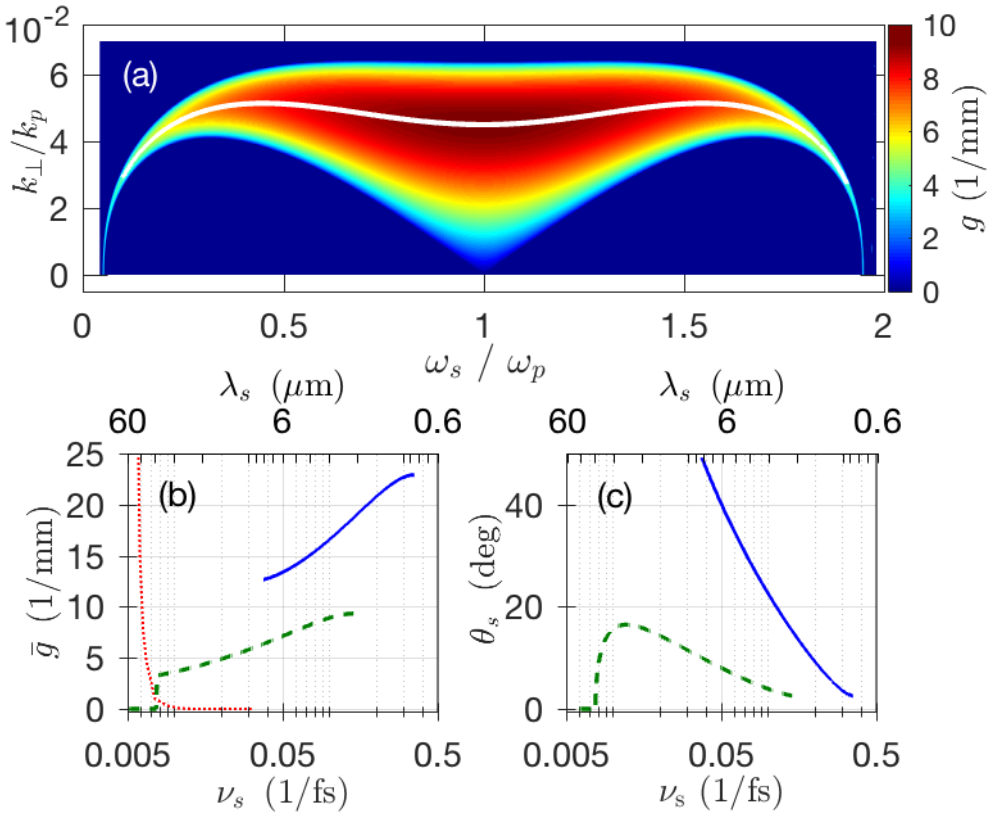


*Figure 3.2: Plane wave amplification in KBr crystal. Panels (a)-(c) correspond to those in Fig. 3.1. In (a) the pump wavelength is $\lambda_p = 2.1\,\mu m$; all other parameters and definitions in panels (a)-(c) are the same as given in the caption of Fig. 3.1.*

$k_\perp = \bar{k}_\perp$, which is equivalent to phase-matching. In other words, KIA is also the generalization to four-wave optical parametric amplification, just with a single (seed) envelope that is extremely broadband, does not rely on the paraxial approximation, and is automatically phase-matched.

Further, $\bar{g}$ increases with pump frequency. For $\lambda_p = 0.85\,\mu$m the gain is still significant at $\lambda_s = 15\,\mu$m. Amplification, $e^{\bar{g}l}$, by more than 4 orders of magnitude can be obtained in a $l = 0.5$ mm long crystal.

For $\lambda_p = 2.1\,\mu$m the gain exists over a narrow spectral range. This is evident from Fig. 3.1(c), where the angle for maximum amplification is plotted for the same two pump wavelengths. At $\lambda_p = 2.1\,\mu$m, $\theta_s$ reaches a maximum near the pump wavelength and then decreases to zero rapidly. This property arises from the functional form of the angle $\theta_s$, due to linear dispersion of $n(\omega)$. Since $\tan^2\theta_s \propto \kappa_\perp^2 \propto \sigma^2 - 1 \approx 2(n_g + n_u\Omega_s/\omega_p)/n_p$. Depending on the material and pump wavelength, the two terms $n_g$ and $n_u\Omega_s/\omega_p$ can have opposite or equal signs, as mentioned above Eq. (2.47). In this particular case, they are of opposite sign and comparable magnitude, so that for decreasing $\nu_s$, $\kappa_\perp^2$ becomes negative. From Eqs. (2.47) and (2.50) we see that then $\bar{k}_\perp = \bar{g} = 0$ so that both gain and $\theta_s$ become zero. A similar behavior can be seen for $\lambda_p = 0.85\,\mu$m, but it is stretched out over a wider spectral range.

In Fig. 3.2, the results for KBr crystals are shown for a pump intensity $I_p = 8$ TW/cm$^2$. The same line styles as in Fig. 3.1 are used. The gain in Fig. 3.2(a) is plotted for $\lambda_p = 2.1\,\mu$m. Unlike in $CaF_2$, using $\lambda_p = 2.1\,\mu$m works well in KBr. Gain exists over a transmission window twice as long as in $CaF_2$, see also Fig. 3.2(b). The maximum gain is still substantial near the edge of the transmission window, see the dotted red line. Amplification of more than four orders of magnitude can be achieved over a crystal length $l = 2$ mm. For $\lambda_p = 0.85\,\mu$m, the gain exists in a narrower spectral range, up to $8\,\mu$m. The reason is clear from Fig. 3.1(c). For $\lambda_p = 0.85\,\mu$m, the angle rapidly increases for increasing $\lambda_s$. As mentioned above for $CaF_2$, this comes from the fact that both terms in $\sigma^2 - 1$ have the same sign. Here, the gain ceases when the denominator in Eq. (2.38) approaches zero for $k_p = \sigma D_u$. By contrast for $\lambda_p = 2.1\,\mu$m, the signs are different and we see similar behavior as in Fig. 3.1(c). Linear dispersion strongly influences KIA and is a crucially important design parameter. The ultrawide frequency range and the large noncollinear angles encountered in Figs. 3.1 and 3.2 emphasize the necessity of our theoretical framework that does not rely on dispersion

expansion and paraxial approximation.

## 3.2 Vector properties of seeded Kerr instability amplification

From Eqs. (2.41) and (2.42) we can explore the vectorial properties of the amplified seed that has been propagated. As an illustrative example, we choose the general initial form for the seed to be

$$\mathbf{v}(z=0) = \begin{bmatrix} a \\ \\ b \end{bmatrix} f(k_x, k_y, \Omega), \tag{3.4}$$

where $a$ and $b$ are real numbers such that $a^2 + b^2 = 1$ and $f(k_x, k_y, \Omega)$ is an arbitrary initial profile of the seed which corresponds to the scalar theory, and is therefore not relevant for this section. Using Eq. (3.4) in Eq. (2.41) we have

$$\mathbf{v}(z) = \hat{P}(z) \begin{bmatrix} a \\ \\ b \end{bmatrix} f(k_x, k_y, \Omega)$$

$$= \begin{bmatrix} p_{11}a + p_{12}b \\ \\ p_{21}a + p_{22}b \end{bmatrix} e^{iK_x z} f(k_x, k_y, \Omega)$$

$$\equiv \mathbf{q} f(k_x, k_y, \Omega) e^{iK_x z}, \tag{3.5}$$

where the $p_{ij}$ are matrix element coefficients of $\hat{P}(z)$ in front of the common factor $e^{iK_x z}$ defined by Eq. (2.42); further $\mathbf{q} = (q_x, q_y)$.

We will now first consider vectorial effects in the pre-exponential factor and then investigate vectorial effects in the exponential gain coefficient. We consider three specific cases for $a$ and $b$ which cover different polarization cases for the initial field; namely: (i) $a = 1$, $b = 0$, (ii) $a = 0$, $b = 1$, and (iii) $a = 1/\sqrt{2}$,

$b = 1/\sqrt{2}$. We begin with case (i) for the material $CaF_2$ where seed frequency coincides with the pump, $\omega_s = \omega_p$. All other parameters are the same as in Fig. 3.1. We need not plot $q_x$ as it is trivially equal to unity since $p_{11} = 1$. We examine only $q_y = p_{21}$ for case (i). As is evident from Fig. 3.3, there is no field

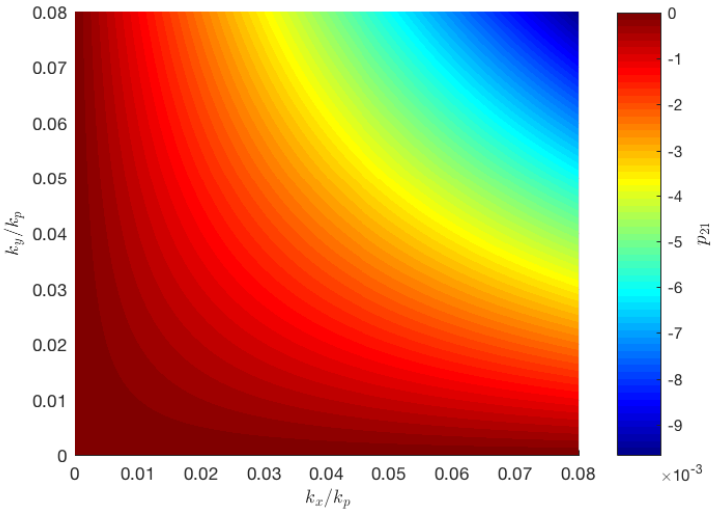


*Figure 3.3: Vectorial effect that causes transverse modulation on the $y-$component of the perturbation due to the propagator of Eq. (3.5) for the case $a = 1$ and $b = 0$.*

present along $k_x = 0$ or $k_y = 0$ in $q_y$, and $q_y$ increases with $k_x$ and $k_y$. Next, we examine the case (ii)

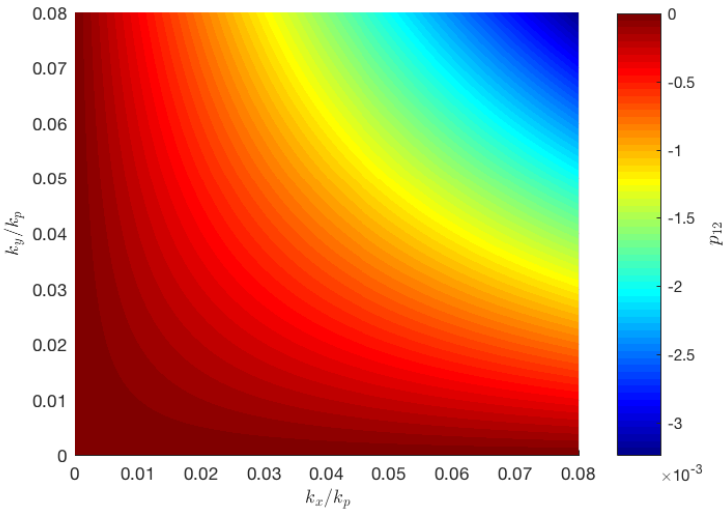


*Figure 3.4: Vectorial effect that causes transverse modulation on the $x-$component of the perturbation due to the propagator of Eq. (3.5) for the case $a = 0$ and $b = 1$.*

where $a = 0$ and $b = 1$. Here, both $q_x$ and $q_y$ exhibit $k_x$ and $k_y$ dependence arising from vectorial effects. In this case, it is clear from Fig. 3.4 that $q_x$ is very similar both qualitatively and quantitatively to $q_y$ of the

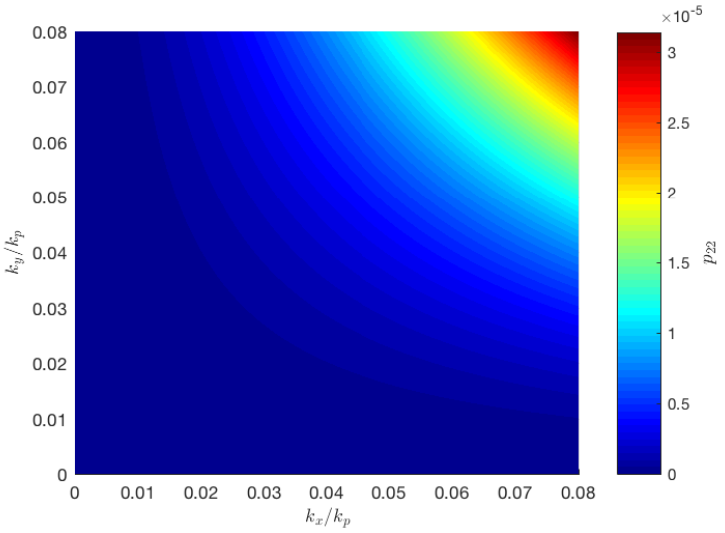


*Figure 3.5: Vectorial effect that causes transverse modulation on the $y-$component of the perturbation due to the propagator of Eq. (3.5) for the case $a = 0$ and $b = 1$.*

previous case. This is reasonable since here $q_x = p_{12}$ which is similar to $q_y = p_{21}$ in case (i). From Fig. 3.5 we see similar qualitative behaviour to Fig. 3.4, but the magnitude is much smaller and the sign is opposite, which is consistent, since the diagonal elements of $\hat{P}(z)$ are positive whereas the off-diagonal elements are negative, see Eq. (2.42). Finally, we consider case (iii), which is a superposition of the previous two cases.

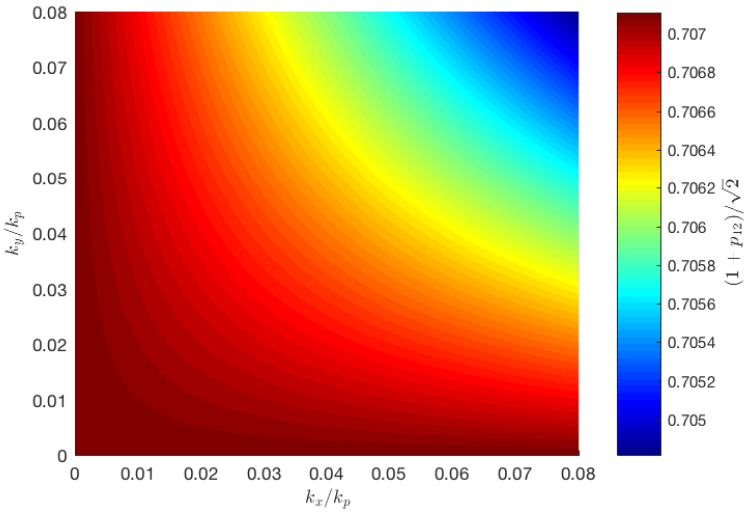


*Figure 3.6: Vectorial effect that causes transverse modulation on the $x-$component of the perturbation due to the propagator of Eq. (3.5) for the case $a = 1\sqrt{2}$ and $b = 1/\sqrt{2}$.*

Again, Figs. (3.6) and (3.7) are qualitatively similar to the previous cases.

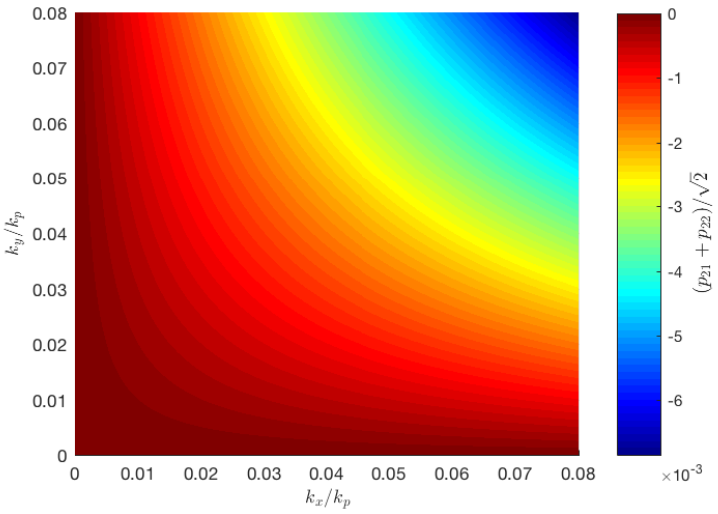


*Figure 3.7: Vectorial effect that causes transverse modulation on the $y-$component of the perturbation due to the propagator of Eq. (3.5) for the case $a = 1/\sqrt{2}$ and $b = 1/\sqrt{2}$.*

In summary, when the seed pulse is polarized along the pump pulse, it is amplified without any additional k-dependence introduced from the prefactor $\mathbf{q}$. Vectorial coupling of KIA leads to a small component of the seed pulse polarized along the orthogonal direction which is distorted by the $k_x$, $k_y$ dependent prefactor. For all other initial conditions, KIA of the seed pulse is weaker and additional $k_x$, $k_y$ dependent is imprinted on the seed pulse due to vectorial effects.

Next, the influence of vectorial effects on the exponential gain is discussed. It is shown that vectorial effects are negligible in the regime where instability gain is possible (discussed in section 3.1). Vectorial effects on the gain from Eq. (2.50) are negligible as long as $r_0 \ll 1$. This is valid as long as the leading order asymmetric term, $r_0$, is small. That is, if

$$|r_0| = \left| \frac{k_x^2 \left( k_v^2 + k_{v(-)}^2 \right)}{k_v^2 k_{v(-)}^2} \right| \ll 1. \tag{3.6}$$

This is valid for most materials, as the instability regime will have ceased before the transverse asymmetry significantly affects the instability gain, see Fig. (3.8), where $r_0$ is plotted. Clearly, the maximum gain is far away from where $r_0$ is significant compared to unity, even for maximized asymmetry, where $k_\perp = k_x$. The instability regime ceases before vectorial effects alter the scalar theory. We conclude that the discussion for

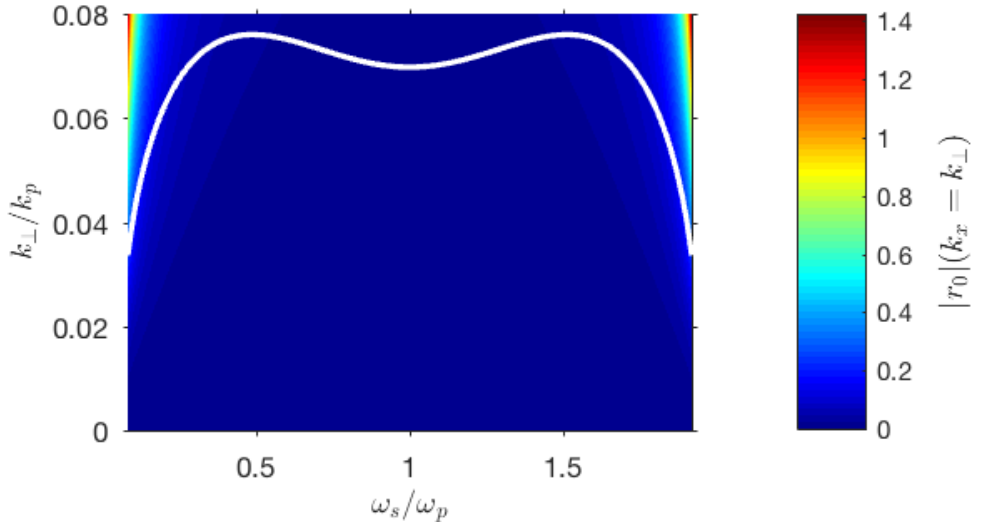


*Figure 3.8: The asymmetric vectorial term, $|r_0|$ (see Eq. (3.6)), is plotted in $CaF_2$ where pump peak intensity $I_p = 50$ $TW/cm^2$. We plot along the line $k_y = 0$ where the asymmetry is maximized at $k_\perp = k_x$. The white line indicates $\bar{k}_\perp$ at which maximum gain $\bar{g} = g(\bar{k}_\perp)$ occurs, see Eq. (2.50).*

KIA in the scalar limit is valid where we assumed $r_0 = 0$ for seed plane waves on the basis of the above two example materials, $CaF_2$ and KBr.

## 3.3 Using seeded Kerr instability amplification to measure the Kerr nonlinearity

Now that we have established that vectorial effects are negligible when considering Kerr instability amplification, we continue with the scalar theory to establish a method to measure the Kerr nonlinearity by means of seeded amplification. We generalize the Kerr nonlinearity to the non-perturbative regime (high intensity), where the Kerr nonlinear index is no longer necessarily a linear function of pump intensity.

A schematic of the measurement concept is shown in Fig. 3.9. Pump and seed pulses are non-collinear, as KIA is maximum for seed pulses with wavevectors on a cone with angle $\theta$ about the pump pulse. The angle for maximum KIA $\bar{\theta}(n_n)$ is a function of the Kerr nonlinearity $n_n = n_2 I_p$ with $n_2$ the Kerr nonlinear index and $I_p$ the pump peak intensity. Repeated measurements of the KIA gain with varying $\theta$ and $I_p$ yields a curve $\bar{\theta}(I_p)$. We find that optimum angle of amplification and Kerr nonlinear index are connected

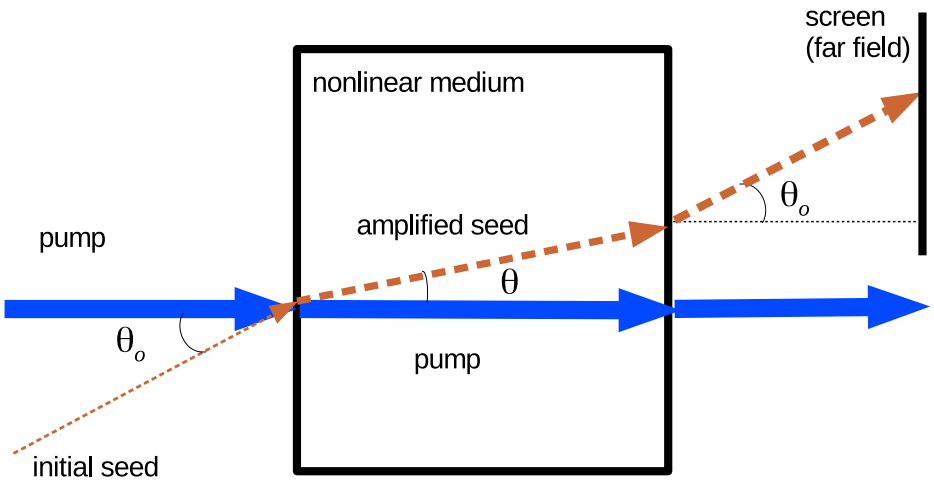


*Figure 3.9: Schematic of the nonlinear index measurement. A strong, monochromatic pump beam (thick solid arrow), interacts non-collinearly with a weak monochromatic seed beam (thin dashed arrow), inclined at an angle $\theta_o$ (angles exaggerated for clarity), both at the same frequency in a nonlinear medium. The seed beam is refracted at an angle $\theta$, and then through nonlinear instability, it is amplified (thicker dashed line). The pump beam remains approximately undistorted. The non-collinear angle is used to calculate the nonlinear index of refraction as shown in this work.*

by an integral relation. With the help of this relation, the functional form and the magnitude of the Kerr nonlinearity can be retrieved from the experimentally measured data $\bar{\theta}(I_p)$.

We start from Maxwell's equations to derive a Kerr nonlinear wave equation for an electric field of the form $E(\mathbf{x},t) = E_p \exp(i\omega_p t - ik_p z) + \varepsilon(\mathbf{x},t) + \text{c.c.}$, a superposition of a cw pump and perturbation $\varepsilon(\mathbf{x},t)$, at the same center frequency, $\omega_p$, where $E_p$ is the constant pump electric field strength, and $k_p$ is the pump wavevector defined below. Usually, the nonlinear polarization vector for a Kerr-type nonlinearity is given by $P^{(3)} = 3\epsilon_0\chi^{(3)}|E|^2E$ for linearly polarized light [8], where $\epsilon_0$ is the vacuum permittivity, and $\chi^{(3)}$ is the Kerr nonlinear susceptibility. Instead, we use the generalized expression, $P^{(3)} = \epsilon_0 f(3\chi^{(3)}|E|^2)E$, where $f$ is a general function of the nonlinear index to be found. We insert $E$ into $P^{(3)}$, neglect higher harmonics, and Taylor expand $f$ to first order, keeping only terms up to $\mathrm{O}(\varepsilon)$

$$P^{(3)} \approx \left[E_p \exp(i\omega_p t - ik_p z) + \varepsilon\right] f\left(n_n\right) + \left[\varepsilon + \varepsilon^* \exp(2i\omega_p t - 2ik_p z)\right] n_n f'(n_n), \tag{3.7}$$

where, as before, $n_n = 3\chi^{(3)}E_p^2 = n_2 I_p$, $n_2$ is the nonlinear refractive index and $I_p$ is the pump intensity.

Here, $f'(n_n)$ is $df/dn_n$ evaluated at $n_n$, and $\varepsilon^*$ denotes the complex conjugate of $\varepsilon$. By setting $r = 0$ in the results (Eqs (2.43−2.50)) from section (2.4), we obtain the scalar KIA theory results. By making the replacements,

$$k_p^2 \to \frac{\omega_p^2}{c^2}\left[n_p^2 + f(n_n)\right], \tag{3.8}$$

$$k_n^2 \to \frac{\omega_p^2 n_n}{c^2} f'(n_n), \tag{3.9}$$

we obtain the scalar theory results valid in the non-perturbative regime. Finally, since we are considering the beams to be monochromatic and coincide at frequency $\omega = \omega_p$, we set $\Omega = 0$ in the results from section (2.4) to obtain

$$K = \pm|k_\perp|\sqrt{k_\perp^2 - 2k_n^2}/(2k_p), \tag{3.10}$$

which is analogous to the work by Bespalov [31]. As before, the argument of the square root in $K$ can become negative; the $-K$ solution leads to exponential growth, with intensity gain

$$g = 2\mathrm{Im(K)} = |\mathrm{k_\perp}|\sqrt{2\kappa_\mathrm{n}^2 - \mathrm{k}_\perp^2}/\mathrm{k_p}. \tag{3.11}$$

The maximum gain occurs for transverse wavevector

$$\bar{k}_\perp = |k_n|, \tag{3.12}$$

and is given by

$$g(\bar{k}_\perp) \equiv \bar{g} = \frac{k_n^2}{k_p}. \tag{3.13}$$

As $\bar{k}_\perp \neq 0$, optimum KIA of the seed beam occurs in a noncollinear setup of seed and pump beam at an

angle

$$\tan\bar{\theta} = \frac{\bar{k}_\perp}{k_p}. \tag{3.14}$$

We insert the definitions for $\bar{k}_\perp$ and $k_p$ into $\tan\bar{\theta}$ to obtain the separable first order differential equation for $f(n_n)$, namely,

$$n_n f'(n_n) - \tan^2\bar{\theta}\left[n^2 + f(n_n)\right] = 0. \tag{3.15}$$

This can be integrated resulting in

$$f(n_n) = n^2\left[\exp\left(\int_0^{n_n}\frac{\tan^2\bar{\theta}(n_n)}{n_n}dn_n\right) - 1\right], \tag{3.16}$$

where $\tan\bar{\theta} \geq 0$, and we required that $f(n_n = 0) = 0$. The Kerr nonlinearity can be measured as follows. At a given pump intensity vary the angle between pump and seed beam until $\bar{\theta}$ is found. Repeat this measurement for a wide range of pump intensities, yielding $\bar{\theta}(I_p)$. Use Eq. (3.16) to retrieve $f(n_n)$ from $\bar{\theta}(n_n)$. Note that the outside angle, $\theta_o$, measured in experiment is found by means of Snell's Law, $\sin\theta_o = n\sin(\arctan(k_\perp/k_p))$. The angle $\bar{\theta}$ refers to the optimum angle for KIA inside the material. In the following we demonstrate how the Kerr nonlinear function $f$ is related to the set of measurements discussed above. We chose a Kerr nonlinear function $f$ that displays saturation behavior as expected from the response of a quantum two level system [8] and that also allows sign change of the Kerr nonlinear index, as was found in recent measurements [37,38]

$$f(n_n) = \frac{n_n - \alpha n_n^2}{(1 + n_n/n_s)^r} \tag{3.17}$$

where $r$ is an arbitrary real number, and $n_s = n_2 I_s$ is the saturation index for saturation intensity $I_s$. The parameter $\alpha = (2-r)/[(4-r)n_s]$ is defined such that $f'(n_n = n_s) = 0$, i.e. $f(n_n = n_s)$ is maximized. The function obeys $f(n_n) \approx n_n$ for $n_n \ll n_s$ and $f(n_n) < 0$ for $\alpha n_n > 1$. Eq. (3.17) has been plotted for various values of $r$ in air, see Fig. 3.10. Panel 3.10(a) shows that as $r$ is increased, $f(n_n)$ is saturated more slowly and hence becomes negative at higher pump intensities. Note that for $r = 1/2$, $f(n_n)$ has similar functional

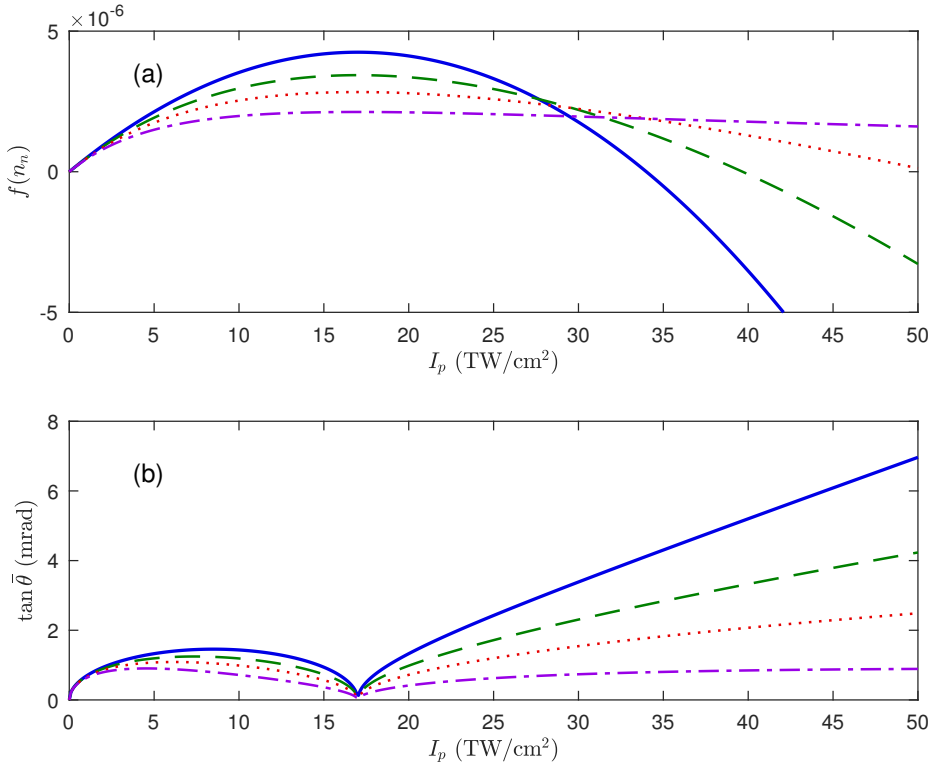


*Figure 3.10: (a) Possible forms for $f(n_n)$ defined by Eq. (3.17) for $r = 0$ (solid blue line), $r = 1/2$ (green dashed line), $r = 1$ (dotted red line), and $r = 2$ (dashed dotted purple line) in air for wavelength $\lambda_p = 0.8$ $\mu m$, $n = 1.0003$ and $n_2 = 5 \times 10^{-19}$ $cm^2/W$, both taken from [8] . Saturation intensity is estimated to be $I_p = 17$ $TW/cm^2$, consistent with Loriot [37, 38] (b) $\tan\bar{\theta}$ defined by Eq. (3.14) corresponding to each case in (a). Linestyles are consistent with r values in (a).*

form to the two-level approximation in the adiabatic following limit [8], with an extra term $\propto \alpha$ that renders $f(n_n) < 0$ eventually. The optimum angle of KIA $\tan(\bar{\theta})$ in Fig. 3.10(a) and the Kerr nonlinear function $f$ in Fig. 3.10(b) are connected by Eq. (3.16). Fig. 3.10 demonstrates that various Kerr nonlinear functions $f$ yield quantitative differences in $\tan\bar{\theta}$, however the overall qualitative behaviour is similar. The angle $\tan(\bar{\theta})$ reaches a local maximum where $f(n_n)$ has an inflection point, where its second derivative is zero; it becomes zero and KIA terminates when $f$ reaches its maximum and the first derivative $f' = 0$. As the maximum gain is connected to $f'$, see Eqs. (3.13) and (3.9), increasing the pump intensity towards this point results in decreasing KIA gain. Beyond this point, KIA starts to increase again with increasing pump intensity. The rate of increase of $\bar{g}$ and $\bar{\theta}$ depends strongly on the functional form of Eq. (3.17). In particular, when the Kerr nonlinear index turns negative (full blue and dashed green curves), the rate of increase of $\tan\bar{\theta}$ is strongest. It grows to values that considerably exceed $\tan\bar{\theta}$ in regime of positive Kerr nonlinearity. Vanishing of KIA presents a hallmark of the end of the intensity dependent growth of the Kerr nonlinearity and of its reversal.

Finally, as absolute intensity measurements are difficult, how can each measured angle $\bar{\theta}(I_p)$ be

assigned its corresponding pump peak intensity? We propose that this can be done in series of relative measurements, where the pump intensity difference between consecutive experiments is known. If this series is extended down to low peak intensities where $f(n_n)$ and $\tan\bar{\theta}$ become linear functions of $I_p$, the measured curve can be extrapolated to zero. The peak intensity can be determined from a measurement of $\bar{\theta}$ concurrently with knowledge of $n_2$ from Z-scan measurements in the perturbative limit of nonlinear optics.

We would like to mention that the vectorial theory may assist the experimental realization of measurements, as one could consider the case (i) discussed in section (3.2), and use the ratio of the intensities of the different transverse polarizations of the amplified seed. That is, the ratio of $|q_y|^2/|q_x|^2 = |q_y|^2 \propto f'(n_n)^2$. It should be noted that the signal for the $y-$polarization would be less intense by an order of $|p_{21}|^2$, which is orders of magnitude smaller than unity, see, for example, Fig. (3.3).

## 3.4 Conclusion

Propagation of optical pulses in Kerr nonlinear materials is inherently unstable and leads to pulse break up resulting in filamentation and the conical emission of wide band radiation. The unstable wave components and conical emission usually grow out of noise. Recently, it was discovered that when the Kerr instability is seeded, substantial amplification occurs long before the pulse break up. It was found that seeded Kerr instability amplification can by used as a wide band amplifier for ultrashort infrared pulses. My thesis builds on this discovery. Whereas the Kerr instability has been so far treated by a scalar analysis, in this thesis I have developed a vector theory of Kerr instability amplification. It shows that KIA is little affected by effects from the vector wave equation. The exponential gain is only modified by vectorial effects in ranges where it is insignificant or does not exist. Vectorial effects exist in the pre-exponential factors and show up as a transverse wavevector dependent modulation of the initial seed profile. This can be avoided by choosing seed and pump pulse polarizations parallel.

The second result, is a novel way to measure the functional form and magnitude of the Kerr nonlinear coefficient in the non-perturbative, high intensity regime of nonlinear optics. It extends the well-known Z-

scan technique to the regime of non-perturbative optics. The measurement relies on finding the angle of maximum amplification between pump and seed pulse as a function of pump intensity. From Kerr instability theory I have developed a relation that connects this angle with the nonlinear refractive index. Whereas in Kerr instability amplification modification of the initial seed pulse due to vectorial effects are undesired, we have found that for the measurement of the Kerr nonlinear index vectorial effects may yield additional information helpful. This and the experimental verification of the proposed mechanism will be subject to future research.

# Bibliography


[1] T. Brabec and F. Krausz, "Nonlinear optical pulse propagation in the single-cycle regime," Physical Review Letters **78**, 3282 (1997).

[2] A. Armaroli and F. Biancalana, "Vector modulational instability induced by parametric resonance in periodically tapered highly birefringent optical fibers," Physical Review A **87**, 063848 (2013).

[3] A. Couairon and A. Mysyrowicz, "Femtosecond filamentation in transparent media," Physics reports **441**, 47-189 (2007).

[4] V. P. Kandidov, O. G. Kosareva, M. P. Tamarov, A Brodeur, S L Chin, "Nucleation and random movement of filaments in the propagation of high-power laser radiation in a turbulent atmosphere," Quantum Electronics **29**, 911-915 (1999).

[5] R. I. Miller, T. G. Roberts, "Laser self-focusing in the atmosphere, Applied Optics **26**, 4570-4575 (1987).

[6] D. Faccio, M. A. Porras, A. Dubietis, F. Bragheri, A. Couairon, and P. Di Trapani, "Conical emission, pulse splitting, and X-wave parametric amplification in nonlinear dynamics of ultrashort light pulses," Physical Review Letters **96**, 193901 (2006).

[7] M. Nesrallah, G. Vampa, G. Bart, P. B. Corkum, C. R. McDonald, and T. Brabec, "Theory of Kerr instability amplification," Optica **5**(3), 271-278 (2018).

[8] R. W. Boyd, "Nonlinear Optics," Third edition, Academic Press, Amsterdam (2008).

[9] J. Shan, T. F. Heinz, "Terahertz radiation from semiconductors," Topics in Applied Physics, **92**, 1-59 (2004).

[10] T. Zhongkan, R. Chandrasekara, T. Y. Chuan, C. Cheng, L. Sha, G. C. Hiang, O. Daniel, and A. Ling, "Generation and analysis of correlated pairs of photons aboard a nanosatellite," Physical Review Applied **5**, 054022 (2016).

[11] P. D. Weidman, A. Herczynski, J. Yu, L. N. Howard, "Experiments on standing waves in a rectangular tank with a corrugated bed," Journal of Fluid Mechanics, **777**, 122-150 (2015).

[12] J. Herrmann, "Theory of Kerr-lens mode locking: role of self-focusing and radially varying gain," Josa b. **11**, 498-512 (1994).

[13] S. V. Suchkov, A. A. Sukhorukov, J. Huang, S. V. Dmitriev, C. Lee, Y. S. Kivshar, "Nonlinear switching and solitons in PT-symmetric photonic systems," Laser & Photonics Reviews **10**, 177-213 (2016).

[14] Y. Chen, E. Rikknen, S. Kaasalainen, J. Suomalainen, T. Hakala , J. Hyypp, and R. Chen, "Two-channel hyperspectral LiDAR with a supercontinuum laser source," Sensors **10**, 7057-7066 (2010).

[15] S. L. Chin, T. -J. Wang, C. Marceau, J. Wu, J. S. Liu, O. Kosareva, N. Panov, Y. P. Chen, J. -F. Daigle, S. Yuan, A. Azarm, W. W. Liu, T. Seideman, H. P. Zeng, M. Richardson, R. Li, Z. Z. Xu,"Advances in intense femtosecond laser filamentation in air," Laser Physics **22**, 1-53 (2012).

[16] J. Kasparian, J. P. Wolf. "Physics and applications of atmospheric nonlinear optics and filamentation," Optics Express **16**, 466-493 (2008).

[17] L. H. Gaabour, Y. E. E. D. Gamal, G. Abdellatif. "Numerical investigation of the plasma formation in distilled water by Nd-YAG laser pulses of different duration," Journal of Modern Physics **3**, 1683 (2012).

[18] S. L. Chin, "Some fundamental concepts of femtosecond laser filamentation," Journal-Korean Physical Society **49**, 281 (2006).

[19] B. G. Bravy, V. M. Gordienko, V. T. Platonenko, "Kerr effect-assisted self-compression in dielectric to single-cycle pulse width and to terawatt power level in mid-IR," Optics Communications **344**, 7-11 (2015).

[20] G. Saathoff, L. Miaja-Avila, M. Aeschlimann and M. M. Murnane and H. C. Kapteyn, "Laser-assisted photoemission from surfaces," Physical Review A **77**, 022903 (2008).

[21] Z. Deng, J. H. Eberly, "Multiphoton absorption above ionization threshold by atoms in strong laser fields," Journal of the Optical Society of America B **2**, 486-493 (1985).

[22] A. D. Piazza, C. Mller, K. Z. Hatsagortsyan, and CH Keitel, "Extremely high-intensity laser interactions with fundamental quantum systems, " Reviews of Modern Physics **84**, 1177 (2012).

[23] L. Plfalvi, "Nonlinear refraction and absorption of Mg doped stoichiometric and congruent LiNbO3". Journal of Applied Physics **95**, 902-908 (2004).

[24] E. W. Van Stryland, M. Sheik-Bahae, "Z-scan measurements of optical nonlinearities," Characterization Techniques and Tabulations for Organic Nonlinear Materials **18**, 655-692 (1998).

[25] P. B. Chapple, J. Staromlynska, R. G. McDuff, "Z-scan studies in the thin-and the thick-sample limits". Journal of the Optical Society of America B **11**, 975-982 (1994).

[26] M. Nesrallah, T. J. Hammond, A. Almalki, G. Bart, C. R. McDonald, T. Brabec, and G. Vampa,"Kerr Instability Amplification," Manuscript in preparation (2018).

[27] H. M. Milchbergb, Y.H. Chen, Y.H. Cheng, N. Jhajj, J. P. Palastro, E. W. Rosenthal, S. Varma, J. K. Wahlstrand, and S. Zahedpour, "The extreme nonlinear optics of gases and femtosecond optical filamentation," Physics of Plasmas **21**, 100901 (2014).

[28] S. G. Johnson, M. Ibanescu, M. A. Skorobogatiy, O. Weisberg, J. D. Joannopoulos, and Y. Fink, "Perturbation theory for Maxwells equations with shifting material boundaries," Physical Review E, **65**, 066611 (2002).

[29] E. Weisstein, "Wolfram Mathworld," url: mathworld.wolfram.com/, (2018).

[30] A. F. Agrawal, M. C. Whitlock. "Mutation load: the fitness of individuals in populations where deleterious alleles are abundant," Annual Review of Ecology, Evolution, and Systematics, **43**, 115-135 (2012).

[31] V. I. Bespalov and V. I. Talanov. "Filamentary structure of light beams in nonlinear liquids," ZhETF Pisma Redaktsiiu **3**, 471 (1966).

[32] E. D. Palik, "Handbook of optical constants of solids II". Academic Press, Boston (1991).

[33] I. H. Malitson, "A redetermination of some optical properties of calcium fluoride," Applied Optics **2**, 1103-1107 (1963).

[34] D. Milam, M. J. Weber, and A. J. Glass, "Nonlinear refractive index of fluoride crystals," Applied Physics Letters **31**, 822-825 (1977).

[35] H. H. Li, "Refractive index of alkali halides and its wavelength and temperature derivatives," J. Phys. Chem. Ref. **5**, 329-528 (1976).

[36] R. DeSalvo, A. A. Said, D. J. Hagan, A. W. Van Stryland, and M. Sheik Bahae, "Infrared to ultraviolet measurement of two-photon absorption and $n_2$ in wide bandgap solilds," IEEE Journal of Quantum Electronics, **32**, 1324-1333 (1996).

[37] V. Loriot, E. Hertz, O. Faucher, and B. Lavorel, "Measurement of high order Kerr refractive index of major air components," Optics Express, **17**, 13429-13434 (2009).

[38] V. Loriot, P. Bejot, W. Ettoumi, Y. Petit, J. Kasparian, S. Henin, E. Hertz, B. Lavorel, O. Faucher, and J. Wolf, "On negative higher-order Kerr effect and filamentation," Laser Phys. **21**, 13191328 (2011).